

การเตรียมและการพิสูจน์เอกลักษณ์ของอนุภาคนาโนซิลิกาไฟโบรอิน



นางสาวกาญจนา อุตัยฉาย

ศูนย์วิทยทรัพยากร


วิทยานิพนธ์นี้เป็นส่วนหนึ่งของการศึกษาตามหลักสูตรปริญญาวิทยาศาสตรมหาบัณฑิต
สาขาวิชาปิโตรเคมีและวิทยาศาสตร์พอลิเมอร์

คณะวิทยาศาสตร์ จุฬาลงกรณ์มหาวิทยาลัย

ปีการศึกษา 2551

ลิขสิทธิ์ของจุฬาลงกรณ์มหาวิทยาลัย

**PREPARATION AND CHARACTERIZATION OF SILK FIBROIN
NANOPARTICLES**



Miss Kanjana Uthaichay

ศูนย์วิทยทรัพยากร

**A Thesis Submitted in Partial Fulfillment of the Requirements
for the Degree of Master of Science Program in Petrochemistry and Polymer Science
Faculty of Science**

Chulalongkorn University

Academic Year 2008

Copyright of Chulalongkorn University

511437

Thesis Title PREPARATION AND CHARACTERIZATION OF SILK
FIBROIN NANOPARTICLES
By Miss Kanjana Uthaichay
Field of Study Petrochemistry and Polymer Science
Thesis Principal Advisor Associate Professor Chuchaat Thammacharoen

Accepted by the Faculty of Science, Chulalongkorn University in Partial Fulfillment
of the Requirements for the Master's Degree

M. Pimolvan Pimpan Deputy Dean for Administrative Affairs,
Acting Dean, The Faculty of Science
(Associate Professor Vimolvan Pimpan, Ph.D.)

THESIS COMMITTEE

Sirirat Kokpol Chairman
(Associate Professor Sirirat Kokpol, Ph.D.)

C. Thammacharoen Thesis Principal Advisor
(Associate Professor Chuchaat Thammacharoen)

Warinthorn Chavasiri Member
(Assistant Professor Warinthorn Chavasiri, Ph.D.)

Sanong Ekgasit Member
(Associate Professor Sanong Ekgasit, Ph.D.)

Jatuphorn External Member
(Associate Professor Jatuphorn Wootthikanokkhan, Ph.D.)

กาญจนา อุทัยฉาย: การเตรียมและการพิสูจน์เอกลักษณ์ของอนุภาคนาโนซิลก์ไฟโบรอิน
(PREPARATION AND CHARACTERIZATION OF SILK FIBROIN
NANOPARTICLES) อ. ที่ปรึกษาวิทยานิพนธ์หลัก: รศ. ชูชาติ ธรรมเจริญ, 74 หน้า.

การเตรียมอนุภาคนาโนซิลก์ไฟโบรอิน โดยวิธีการตกตะกอนของสารละลายซิลก์ไฟโบรอิน
ในตัวทำละลายอินทรีย์ ได้แก่ เมทานอล เอทานอล และไอโซโพรพานอล เป็นวิธีการเตรียมที่มี
ขั้นตอนง่ายๆ ไม่ยุ่งยาก ไม่ต้องใช้ความร้อน สามารถควบคุมโครงสร้างทุดิภูมิภาคของอนุภาคนาโน
ซิลก์ไฟโบรอินได้ด้วยตัวทำละลายอินทรีย์ ขนาดและรูปร่างของอนุภาคนาโนซิลก์ไฟโบรอินที่
เตรียมได้ตรวจสอบโดยใช้กล้องจุลทรรศน์อิเล็กตรอนแบบส่องกราด ได้ทำการศึกษาปัจจัยต่างๆ
เพื่อเตรียมอนุภาคนาโนซิลก์ไฟโบรอินที่มีขนาดเล็ก ซึ่งวิธีการนี้สามารถเตรียมอนุภาคนาโนซิลก์
ไฟโบรอินทรงกลมมีขนาด 90 ถึง 100 นาโนเมตร การวิเคราะห์เชิงโมเลกุลของเส้นใยไหมไฟ
โบรอิน สารละลายซิลก์ไฟโบรอิน ซิลก์ไฟโบรอินฟิล์ม และอนุภาคนาโนซิลก์ไฟโบรอินที่เตรียม
ได้โดยใช้เทคนิคเอทีอาร์เอฟทีไออาร์ไมโครสเปกโทรสโกปี พบว่าโครงสร้างทุดิภูมิภาคของอนุภาค
นาโนซิลก์ไฟโบรอินที่ได้จากการตกตะกอนในเมทานอลมีความเป็นผลึกมากกว่า โครงสร้างทุดิ
ภูมิภาคของอนุภาคนาโนซิลก์ไฟโบรอินที่ได้จากการตกตะกอนในเอทานอล และไอโซโพรพานอล
แสดงให้เห็นว่าเราสามารถควบคุมโครงสร้างทุดิภูมิภาคของอนุภาคนาโนซิลก์ไฟโบรอินได้ด้วยตัวทำ
ละลายอินทรีย์ อนุภาคนาโนซิลก์ไฟโบรอินสามารถนำมาประยุกต์ใช้ในการเป็นตัวรองรับอนุภาค
นาโนเงินได้ จากการศึกษาพบว่าอนุภาคนาโนเงินสามารถกระจายตัวและเกาะอยู่บนอนุภาคนาโน
ซิลก์ไฟโบรอินได้ดี

ศูนย์วิทยทรัพยากร

จุฬาลงกรณ์มหาวิทยาลัย

สาขาวิชา.....ปีโคเรเคมีและวิทยาศาสตร์พอลิเมอร์.....ลายมือชื่อนิสิต.....กัญญา.....อุทัยฉาย

ปีการศึกษา.....2551.....ลายมือชื่ออาจารย์ที่ปรึกษาวิทยานิพนธ์หลัก.....ช. ธรรมเจริญ.....

4972217723: MAJOR PETROCHEMISTRY AND POLYMER SCIENCE

KEYWORD: SILK FIBROIN NANOPARTICLES / SECONDARY STRUCTURE /
PROTEIN / ATR FT-IR MICROSPECTROSCOPY

KANJANA UTHAICHAY: PREPARATION AND CHARACTERIZATION
OF SILK FIBROIN NANOPARTICLES. THESIS PRINCIPAL ADVISOR:
ASSOC. PROF. CHUCHAAT THAMMACHAROEN, 74 pp.

Silk fibroin nanoparticles were prepared by precipitating silk fibroin solution in organic solvents (methanol, ethanol, and *iso*-propanol). The secondary structure of silk fibroin nanoparticles was controlled by organic solvent. The size and morphology of the silk fibroin nanoparticles were characterized by scanning electron microscopy (SEM). Silk fibroin nanoparticles were prepared. The results indicated that the silk fibroin nanoparticles have spherical shape with particles sizes in the range 90-100 nm. The molecular characteristics of single silk fiber, silk fibroin solution, silk fibroin films, and silk fibroin nanoparticles were investigated by ATR FT-IR microspectroscopy. The technique gives molecular information of native single silk fiber without sample destruction. The results indicated that the secondary structure of silk fibroin nanoparticles precipitated in methanol were rich in β -sheet structure compared to those prepared from ethanol and *iso*-propanol. Silk fibroin nanoparticles can apply for silver nanoparticles deposition. Silver nanoparticles are well dispersed and well deposited on silk fibroin nanoparticles.

Field of student ..Petrochemistry and Polymer Science.. Student's signature...*Kanjana Uthachay*..
Academic year ...2008... Principal Advisor's signature...*C. Thammachaoen*..

ACKNOWLEDGEMENTS

I would like to express my sincere gratitude to my thesis advisor, Associate Professor Chuchaat Thammacharoen and Associate Professor Dr. Sanong Ekgasit who always provide the useful guidance, suggestion, encouragement, understanding as well as patiently practices my technical skill during the whole research.

I would like to thank Associate Professor Dr. Sirirat Kokpol, Associate Professor Dr. Jatuphorn Wootthikanokkhan, Assistant Professor Dr. Warinthorn Chavasiri, and Associate Professor Dr. Sanong Ekgasit for usefully substantial suggestions as the thesis committee.

The authors would like to acknowledge Mr. Wonchalerm Rungswang, and Associate Professor Dr. Suwabun Chirachanchai for the morphological characterization using transmission electron microscopy technique, Mr. Prateep Meesilpa, Director of The Queen Sirikit Institute of Sericulture, Office of the Permanent Secretary for Agriculture and Cooperatives, Ministry of Agriculture and Cooperatives for silk fiber supply, and National Center of Excellence for Petroleum, Petrochemicals and Advanced Materials, NCE-PPAM and The Commission on Higher Education for partial financial support.

Finally, I would like to thank my wonderful parents and the endearing family for their love, understanding, encouragement, and overwhelmingly support.

ศูนย์วิทยทรัพยากร
จุฬาลงกรณ์มหาวิทยาลัย

CONTENTS

	Page
ABSTRACT (IN THAI).....	iv
ABSTRACT (IN ENGLISH).....	v
ACKNOWLEDGEMENTS.....	vi
CONTENTS.....	vii
LIST OF FIGURES.....	x
LIST OF TABLES.....	xiv
LIST OF ABBREVIATIONS.....	xv
LIST OF SYMBOLS.....	xvi
CHAPTER I INTRODUCTION.....	1
1.1 Silk fibroin.....	1
1.1.1 Silk fibers structure.....	1
1.1.2 Silk fibroin structure.....	2
1.1.2.1 Primary structure.....	3
1.1.2.2 Secondary structure.....	3
1.1.2.3 Tertiary structure.....	3
1.1.2.4 Quaternary structure.....	3
1.1.3 Secondary structure of silk fibroin protein.....	3
1.1.4 Chemical composition of silk fibroin protein.....	6
1.2 Silk fibroin nanoparticles.....	7
1.3 Preparation of silk fibroin nanoparticles.....	7
1.4 Characterization of silk fibroin by ATR FT-IR microspectroscopy....	8
1.5 The objectives of this research.....	9
1.6 The scopes of this research.....	9
CHAPTER II THEORETICAL BACKGROUND.....	10
2.1 Fundamentals of spectroscopy.....	10

	Page
2.2 Attenuated Total Reflection Fourier Transform Infrared (ATR FT-IR) Spectroscopy.....	12
2.2.1 Principle of light reflection and refraction.....	13
2.2.2 Internal Reflection Element (IRE).....	14
2.2.3 ATR spectral intensity and penetration depth.....	14
 CHAPTER III EXPERIMENTAL SECTION.....	 16
3.1 Materials	16
3.2 Experimental section.....	16
3.2.1 Preparation of <i>Bombyx mori</i> silk fibroin solution.....	17
3.2.2 Preparation of the silk fibroin films.....	17
3.2.3 Preparation of the precipitating solution.....	17
3.2.4 Preparation of silk fibroin nanoparticles.....	18
3.2.5 The deposition of silver nanoparticles on silk fibroin nanoparticles.....	18
3.2.4 Preparation of silk fibroin nanoparticles.....	18
3.3 Characterization of silk fibroin nanoparticles.....	19
3.3.1 ATR FT-IR microspectroscopy	19
3.3.1.1 Instrument.....	19
3.3.1.2 Default Spectral Acquisition Parameter.....	20
3.3.2 Scanning electron microscopy	21
3.3.3 Transmission electron microscopy	22
3.3.4 UV-Visible spectroscopy	23
 CHAPTER IV RESULTS AND DISCUSSION.....	 25
4.1 The effect of concentration of NaCl in silk fibroin solution for precipitation in methanol	25
4.2 The effect of silk fibroin concentration on precipitation in organic solvents.....	27

	Page
4.3 Chemical information of silk fibroin.....	30
4.3.1 Chemical information of silk fibroin fiber.....	31
4.3.2 Chemical information of silk fibroin nanoparticles precipitated in organic solvents.....	33
4.4 The secondary structure analysis of silk fibroin by ATR FT-IR Microspectroscopy.....	37
4.4.1 Comparison of virgin silk fiber and degummed silk fiber (silk fibroin fiber).....	37
4.4.2 Comparison of the silk fibroin fiber, the silk fibroin solution, the silk films, and the silk fibroin nanoparticles.....	43
4.4.3 Comparison of the single silk fibroin fiber and the silk fibroin nanoparticles.....	45
4.4.4 Comparison of silk fibroin nanoparticles precipitated from different organic solvents.....	50
4.5 The deposition of silver nanoparticles on silk fibroin nanoparticles.....	55
4.5.1 TEM images of silver nanoparticles and silver-deposited silk fibroin nanoparticles.....	61
4.5.2 Comparison of silk fibroin nanoparticles and silver-deposited silk fibroin nanoparticles.....	63
 CHAPTER V CONCLUSIONS.....	 68
 REFERENCES.....	 70
 CURRICULUM VITAE.....	 74

LIST OF FIGURES

Figure	Page
1.1 Structure of the silk fiber.....	2
1.2 Four levels of protein structure.....	2
1.3 The antiparallel and parallel β -pleated sheet structure.....	4
1.4 A single β -strand structure.....	4
1.5 The β -turn structure.....	5
1.6 The secondary structure: (a) the α -helical structure and (b) random coil structure.....	5
2.1 Propagation of a linearly polarized electromagnetic wave in the direction of propagation. Electric (E) and magnetic (H) vectors are always perpendicular to each other and to the direction of propagation.	10
2.2 Interactions of light with matter.....	11
2.3 Ray tracing under total internal reflection.....	13
2.4 Reflection and refraction of a plane wave at a dielectric interface based on Snell's law.....	13
2.5 IRE configurations commonly used in ATR experimental setups: (a) Single reflection variable-angle hemispherical crystal and (b) Multiple reflection single-pass crystal.....	14
3.1 The dialysis tubing of silk fibroin solution.....	17
3.2 ATR FT-IR microspectroscope: (A) Continuum TM infrared microscope attached to the Nicolet 6700 FT-IR spectrometer, (B) the slide-on Ge μ IRE is fixed on the position of slide-on housing on the infrared objective, and (C) Homemade slide-on Ge μ IRE.....	21
3.3 JEOL JSM-6480LV analytical scanning electron microscope.....	22
3.4 Hitachi zero A H-7650 transmission electron microscope.....	22
3.5 Toshiba USB4000 ocean optics portable UV-Visible spectrometer.....	23
4.1 SEM images of silk fibroin particles at different concentrations of NaCl: (a) 0 M, (b) 0.015 M, (c) 0.05 M, and (d) 0.25 M.	26

Figure	Page
4.2 SEM images of silk fibroin particles at different silk fibroin concentrations: (a1) 16.6%, (a2) 25%, (a3) 50% v/v. Silk fibroin solutions were precipitated in methanol, (b1) 16.6%, (b2) 25%, (b3) 50% v/v. Silk fibroin solutions were precipitated in ethanol, (c1) 16.6%, (c2) 25%, (c3) 50% v/v. Silk fibroin solutions were precipitated in <i>iso</i> -propanol.....	28
4.3 Photograph of silk fibroin particles at different silk fibroin concentrations: (a) silk fibroin particles precipitated in methanol, (b) silk fibroin particles precipitated in ethanol, and (c) silk fibroin particles precipitated in <i>iso</i> -propanol.....	29
4.4 ATR FT-IR spectrum of single silk fibroin fiber acquired by the slide-on Ge μ IRE.....	31
4.5 Derivative spectra of single silk fibroin fiber: (A) first-derivative and (B) second-derivative.....	33
4.6 ATR FT-IR spectrum of silk fibroin nanoparticles precipitated in methanol by the slide-on Ge μ IRE	34
4.7 ATR FT-IR spectrum of silk fibroin nanoparticles precipitated in ethanol by the slide-on Ge μ IRE.....	34
4.8 ATR FT-IR spectrum of silk fibroin nanoparticles precipitated in <i>iso</i> -propanol by the slide-on Ge μ IRE	35
4.9 Comparison of ATR FT-IR spectra of silk: (A) sericin gum, (B) single virgin silk fiber, and (C) single degummed silk fiber. The spectra were acquired by the Ge slide-on IRE.....	37
4.10 ATR FT-IR spectra of a single silk fiber in the Amide I region (bottom) with the corresponding second-derivative spectra (top): (A) Virgin silk fiber and (B) Degummed silk fiber	40
4.11 Curve fitting of spectrum of single virgin silk fiber in the Amide I region.....	41
4.12 Curve fitting of spectrum of single degummed silk fiber in the Amide I region.....	42

Figure	Page
4.13 Comparison of ATR FT-IR spectra of silk: (A) silk fibroin fiber, (B) silk fibroin solution (before dialysis), (C) silk fibroin films, and (D) silk fibroin nanoparticles. The spectra were acquired by the Ge slide-on IRE. FT-IR spectra of water in Figure 4.13 (B) was added for comparison.....	44
4.14 Normalized ATR FT-IR spectra of silk fibroin fiber at three different positions.....	45
4.15 Normalized ATR FT-IR spectra of silk fibroin nanoparticles precipitated in methanol	46
4.16 Normalized ATR FT-IR spectra of silk fibroin nanoparticles precipitated in ethanol.....	46
4.17 Normalized ATR FT-IR spectra of silk fibroin nanoparticles precipitated in <i>iso</i> -propanol.....	47
4.18 ATR FT-IR spectra of silk: (a) silk fibroin fiber, (b) silk fibroin nanoparticles precipitated in methanol, (c) silk fibroin nanoparticles precipitated in ethanol, and (d) silk fibroin nanoparticles precipitated in <i>iso</i> -propanol.....	48
4.19 Curve fitting of spectrum of silk fibroin nanoparticles in the Amide I region	49
4.20 ATR FT-IR spectra of silk: (a) silk fibroin nanoparticles precipitated in methanol, (b) silk fibroin nanoparticles precipitated in ethanol, and (c) silk fibroin nanoparticles precipitated in <i>iso</i> -propanol.....	50
4.21 Curve fitting of spectrum of silk fibroin nanoparticles precipitated with methanol in the Amide I region.....	52
4.22 Curve fitting of spectrum of silk fibroin nanoparticles precipitated with ethanol in the Amide I region.....	53
4.23 Curve fitting of spectrum of silk fibroin nanoparticles precipitated with <i>iso</i> -propanol in the Amide I region.....	53
4.24 Curve fitting of spectrum of silk fibroin films in the Amide I region....	54

Figure	Page
4.25 Photograph of silver nanoparticles at different concentrations deposited on silk fibroin nanoparticles: (a) 50 ppm, (b) 100 ppm, and (c) 200 ppm.....	56
4.26 TEM images of silver nanoparticles colloidal solution.....	56
4.27 The UV-Visible absorption spectra of silver nanoparticles: (a) Silk fibroin nanoparticles, (b) before silver nanoparticles were added, and (c) after silver nanoparticles were added.....	57
4.28 The calibration curve of UV-Visible absorption spectra of silver nanoparticles: (a) 10.0 ppm, (b) 8.00 ppm, (c) 6.5 ppm, (d) 5.0 ppm, (e) 3.5 ppm, (f) 2.5 ppm, (g) 1.5 ppm, (h) 0.5 ppm, and (i) 0.05 ppm....	58
4.29 Plot of intensity at absorption maxima against silver nanoparticles concentrations (ppm).....	58
4.30 The UV-Visible absorption spectra released silver nanoparticles from silk fibroin nanoparticles: (a) 50 ppm, (b) 100 ppm, and (c) 200 ppm...	61
4.31 TEM images of silk fibroin nanoparticles and silver nanoparticles colloidal solution.....	62
4.32 TEM images of silk fibroin nanoparticles deposited with silver nanoparticles: (a) and (b) deposited at 50 ppm; (c) and (d) deposited at 100 ppm; and (e) and (f) deposited at 200 ppm.....	62
4.33 ATR FT-IR spectra of silk fibroin nanoparticles: (A) no deposition, (B) silver-deposited at 50 ppm (C) silver-deposited at 100 ppm, and (D) silver-deposited at 200 ppm, respectively.....	64
4.34 Curve fitting of spectrum of silver-deposited at 50 ppm in the Amide I region.....	65
4.35 Curve fitting of spectrum of silver-deposited at 100 ppm in the Amide I region.....	65
4.36 Curve fitting of spectrum of silver-deposited at 200 ppm in the Amide I region	66
4.37 The proposed mechanism of silver nanoparticles inserted into the silk fibroin structures.....	67

LIST OF TABLES

Table	Page
1.1 Amino acid composition of <i>Bombyx mori</i> fibroin.....	6
4.1 The particles size of silk fibroin particles at different concentration of NaCl	26
4.2 The particles size of silk fibroin particles at different silk fibroin concentrations.....	27
4.3 Peak assignments of single silk fibroin fiber.....	32
4.4 Peak assignments of silk fibroin nanoparticles.....	35
4.5 Peak assignments of single silk fiber and degummed single silk fiber...	39
4.6 The secondary structure of single virgin silk fiber and single degummed silk fiber.....	42
4.7 The secondary structure analysis of silk fibroin fiber and silk fibroin nanoparticles.....	49
4.8 The secondary structure analysis of silk fibroin nanoparticles precipitated with different organic solvents.....	55
4.9 The silver nanoparticles concentration (The sample was twenty times dilution with deionized water).....	59
4.10 Weight of silver nanoparticles deposited on silk fibroin nanoparticles (The sample was twenty times dilution with deionized water).....	60
4.11 Weight of silver nanoparticles deposited on silk fibroin nanoparticles...	60
4.12 Weight of silver nanoparticles released from silk fibroin nanoparticles.	61
4.13 The secondary structure analysis of silver-deposited silk fibroin nanoparticles.....	66

LIST OF ABBREVIATIONS

Ala	: Alanine
ATR	: Attenuated total reflection
C	: Carbon
Da	: Dalton
FT-IR	: Fourier transform infrared
Ge	: Germanium
Gly	: Glycine
IRE	: Internal reflection element
KBr	: Potassium bromide
kV	: Kilovolt (10^3 V)
LiBr	: Lithium bromide
M	: Molar
MCT	: Mercury-cadmium-telluride
MSEF	: Mean square electric field
MSEvF	: Mean square evanescent field
MWCO	: Molecular weight cut off
m	: Medium band
mg	: Milligram (10^{-3} g)
mL	: Milliliter (10^{-3} L)
NaCl	: Sodium chloride
nm	: Nanometer (10^{-9} m)
ppm	: Part per million
s	: Strong band
SEM	: Scanning electron microscopy
Ser	: Serine
TEM	: Transmission electron microscopy
v	: Volume
wt	: Weight
w	: Weak band
ZnSe	: Zinc selenide

LIST OF SYMBOLS

k	: Kilo (10^3)
β	: Beta
α	: Alpha
μ	: Micro (10^{-6})
k_2	: Absorption index of the sample
n_1	: Refractive index of the dense medium (IRE)
n_2	: Refractive index of the sample
I	: Light intensity
I_0	: Intensity of incident beam
I_R	: Intensity of reflected beam
I_S	: Intensity of scattered beam
I_T	: Intensity of transmitted beam
I_A	: Intensity of absorbed beam
θ	: Angle of incidence
θ_c	: Critical angle
A	: Absorbance
R	: Reflectance
c	: Concentration
ϵ	: Absorption coefficient
ν	: Wavenumber
l	: Film thickness
d_p	: Penetration depth
$^{\circ}\text{C}$: Degree Celsius
λ	: Wavelength

ศูนย์วิจัยทรัพยากร
จุฬาลงกรณ์มหาวิทยาลัย

CHAPTER I

INTRODUCTION

Silk fibers are the natural protein polymer. They are produced by the silkworm so as to form cocoon. The main component of silk fibers consists of two proteins: sericin and fibroin. The fibroin content is 66.5-73.5 wt%, and the sericin content is 26.5-33.5 wt% of the total silk fiber [1]. Fibroin is mainly long fibers, which are coated with sericin. Silk fibers also contain minor amounts of impurities such as fats, waxes, dyes, and mineral salts.

1.1 Silk fibroin

Silk fibroin composes of heavy chains (350 kDa) and light chains (25 kDa) [2]. Two components are linked by disulfide linkages. The heavy chains contain the Gly, Ala, Ser, and Tyr residues [3]. The degree of crystallinity of silk fibroin fiber is related to antiparallel β -sheet crystalline, which are aligned along the fiber axis.

1.1.1 Silk fibers structure

The silk fiber has two main components called *fibroin* and *sericin*. Fibroin is mainly a long fiber and sericin is silk gum. The raw silk fiber consists of two fibroin strands. Sericin acts as gum for adhesive the twin fibroin strands. Nanofibrils are packed together to form the microfibrils and several microfibrils produce a single fibroin strand. The structure of single silk fiber is shown in Figure 1.1.

จุฬาลงกรณ์มหาวิทยาลัย

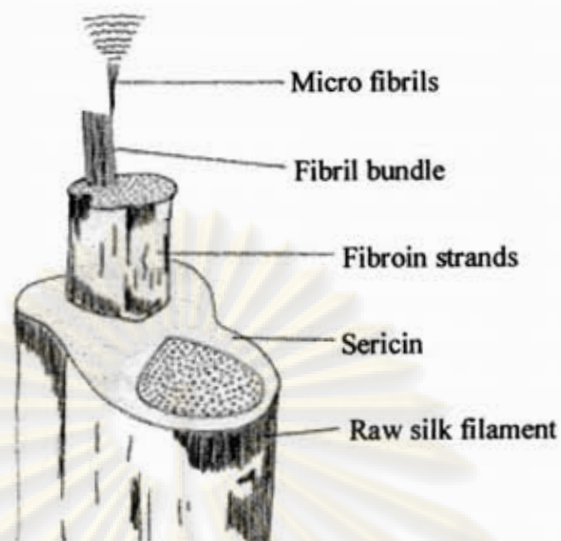


Figure 1.1 Structure of the silk fiber [4].

1.1.2 Silk fibroin structure

Silk fibroin protein is classified to four levels of protein structure.

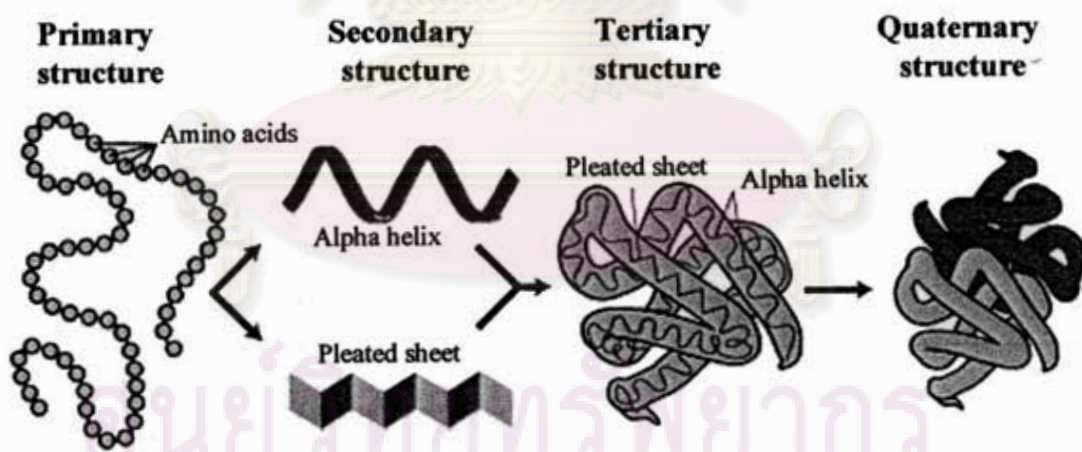


Figure 1.2 Four levels of protein structure [5].

1.1.2.1 Primary structure

Primary structure refers to amino acid sequence in the polypeptide chains. The repeating units of silk fibroin are composed of poly glycine and alanine blocks. Their sequences are $-(\text{Gly-Ala-Gly-Ala-Gly-Ser})_n$. The silk protein amino acids in the sequence are non-polar side groups.

1.1.2.2 Secondary structure

Secondary structure is the initial arrangement of the linear polypeptide. The common structure is the β -pleated sheet and α -helix structure.

1.1.2.3 Tertiary structure

Tertiary structure refers to three-dimensional arrangement of the polypeptide chains, which many secondary structures are organized into multiple domains. The domains are composed of the globular structure protein, which the β -pleated sheet and α -helix structure are interacted via side group of non-polar amino acid with van der Waals force.

1.1.2.4 Quaternary structure

Quaternary structure refers to the complex of the two or more globular/tertiary structure proteins.

1.1.3 Secondary structure of silk fibroin protein

Silk fibroin consists of two phases: crystalline and non-crystalline regions. The crystalline regions are formed by the repetitive sequences of hydrophobic blocks $((\text{Gly-Ala-Gly-Ala-Gly-Ser})_n)$ and identified as the β -pleated sheet structure as shown in Figure 1.3 [6]. The β -pleated sheet consists of the multiple β -strands, which refers to a single continuous polypeptide backbone of amino acids. The β -strands structures are shown in Figure 1.4. The multiple of adjacent β -strands are aligned along in the same direction from N terminus or C terminus to the other and formed hydrogen bond

between each other, which is referred to parallel β -pleated sheet. The multiple of adjacent β -strands are aligned along the opposite direction from N terminus or C terminus to the other and form hydrogen bond between each other, which is referred to antiparallel β -pleated sheet. The β -turn structure is found at turns of β -pleated sheet structure, which composed of four consecutive residues. The β -turn structure is classified to two types. Type I refers to the β -turn having side chain of amino acid is the same direction and Type II refers to side chain of amino acid is opposite direction as shown in Figure 1.5

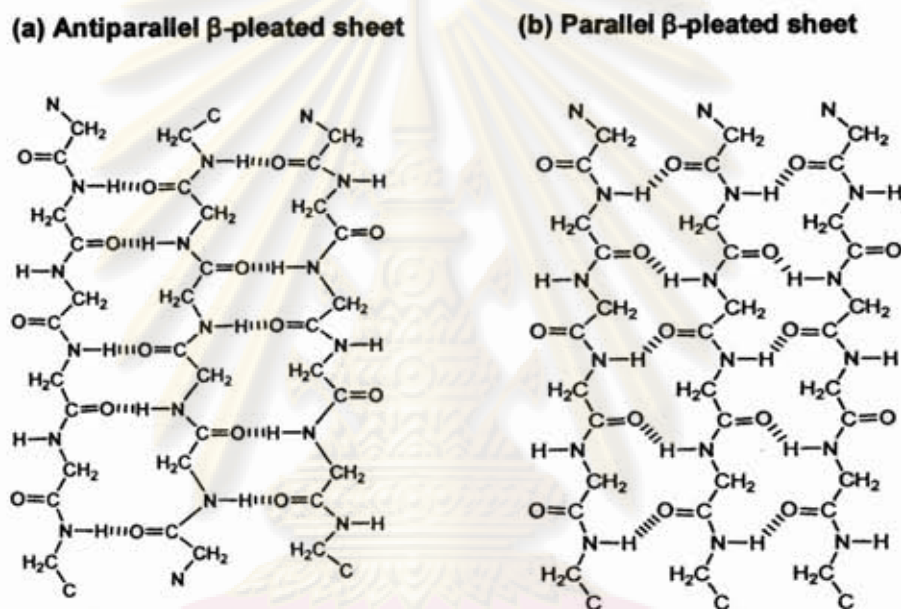


Figure 1.3 The antiparallel and parallel β -pleated sheet structure.



Figure 1.4 A single β -strand structure.

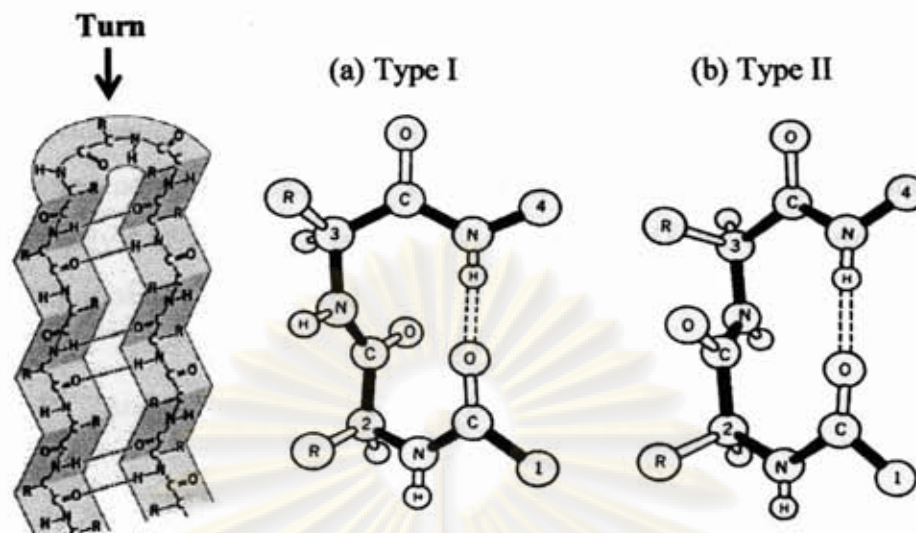


Figure 1.5 The β -turn structure [7].

The non-crystalline regions are identified as the α -helical structure and the random coil or amorphous structure is shown in Figure 1.6. The α -helical structure refers to the polypeptide chain twists itself to spiraling and form intra-molecular hydrogen bond.

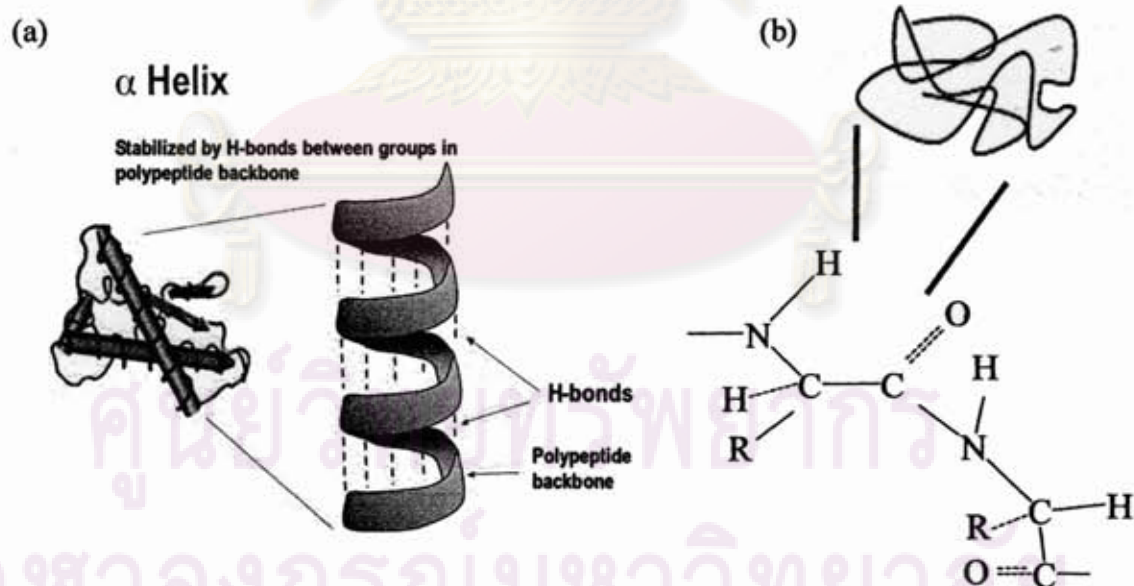


Figure 1.6 The secondary structure: (a) the α -helical structure and (b) random coil structure [8].

1.1.4 Chemical composition of silk fibroin protein

The *Bombyx mori* silk fibroin protein consists of more than 16 amino acids. The major amino acid components are glycine, alanine, and serine (3:2:1 molar ratio) approximately 44.6%, 29.4%, and 12.1%, respectively [1, 9]. The normal amino acid compositions of silk *Bombyx mori* fibroin are shown in Table 1.1.

Table 1.1 Amino acid composition of *Bombyx mori* fibroin [10].

Amino acid	Composition (residues/1000 residues)
Glycine	446
Alanine	294
Serine	121
Tyrosine	51.7
Aspartic acid	13
Arginine	4.7
Histidine	1.4
Glutamic acid	10.2
Lysine	3.2
Valine	22
Leucine	5.3
Isoleucine	6.6
Phenylalanine	6.3
Proline	3.6
Threonine	9.1
Methionine	1
Tryptophan	1.1
Cystein	2

1.2 Silk fibroin nanoparticles

Silk fibroin is the natural protein polymer as well as biomaterials. Silk biomaterials are biocompatible for human tissues and harmless to human body. Silk fibroin can regenerate to various forms such as powder, film, gel, and filament.

The size of silk fibroin nanoparticles are in the range of approximately 1-100 nm. They used in the field of life science such as useful additive for cosmetics, hair care production, anti-UV skincare products, and used as matrices for drug delivery system [6, 11]. In 2007, Wang et al. [12] prepared silk microspheres under mild processing conditions for encapsulation and controlled release protein drug in active forms. The microspheres were found to be small in size (less than 2 μm). Secondary structure is a β -sheet structure. In 2003, Hino et al. [13] prepared silk microspheres by spray-drying silk fibroin aqueous solution containing theophylline as a model drug with a small amount of ethanol. The microspheres were found that they have the mean particles sizes of 5 μm and the secondary structure changed to β -sheet structure.

1.3 Preparation of silk fibroin nanoparticles

In general, silk fibroin nanoparticles were produced by dividing silk fibers with mechanical pulverization such as pin mill or jet mill or by spray-drying technique. However, both techniques are not suitable for preparation of silk fibroin nanoparticles, since silk fibers have high tensile strength. They are difficult to crush by pulverization. Therefore, silk fiber must be treated with alkaline aqueous solution until their tensile strength becomes approximately 0.05 gram/denier [14]. This technique is not suitable because it contains three step processes. The crush and the treatment takes very long time (1-4 hours) for silk fiber. Spray-drying technique is a high temperature technique. High temperatures prohibit silk fibroin nanoparticles getting used for protein drug delivery and secondary structures are difficult to control. In 2002, Yeo et al. [15] prepared silk fibroin microspheres particles by spray-drying silk fibroin aqueous solution. The microspheres were spherical in shape and the particles size of $2 \pm 10 \mu\text{m}$. Secondary structure changed from random coil to β -sheet structure during spray dry process. In 2000, Nam et al. [16] prepared regenerated silk fibroin by freezing and lyophilizing silk fibroin solution. The freezing temperature

and the type of alcohol addition affected the morphological and secondary structure. Secondary structure changed from random coil to β -sheet, when hydrophilic alcohol was added to silk fibroin solution. Hydrophobic alcohol did not change the conformation of silk fibroin into β -sheet structure as the silk fibroin remained in a random coil conformation. Regenerated silk fibroins were lump-like or sheet-like shape when added hydrophobic alcohol and they were fine powder in shape when added hydrophilic alcohol. In 2005, Li et al. [17] prepared nanoscale silk particles from silk fibroin fiber by three-steps pulverization techniques. The particles size of the first and the second pulverized silk powders are approximately from 1-20 μm and from 0.1-5 μm , respectively. The particles sizes of the third pulverization were less than 100 nm and the particles are spherical.

In this research, a simple technique for the simplification of the preparation of silk fibroin nanoparticles by precipitation was developed. This method can controlled the secondary structure of silk nanoparticles depending on the type of organic solvents. Silk fibroin solution was precipitated in organic solvent at room temperature.

1.4 Characterization of silk fibroin by ATR FT-IR microspectroscopy

Fourier transform infrared (FT-IR) spectroscopy is a technique to characterize molecular orientation and molecular vibration of protein such as silk fibroin [18]. This technique is the measurement of the wavelength and intensity of the absorption of infrared light interacting by functional groups of a sample [19]. FT-IR spectroscopy can be analyzed in many modes such as transmission and reflection modes. Attenuated total reflection (ATR) technique is one of reflection modes. ATR FT-IR spectroscopy is the surface analysis and is a non-destructive technique. This technique was used to investigate the secondary structure changes in silk fibroin during the preparation of silk fibroin nanoparticles. The technique also provides molecular characteristics of native single silk fiber without sample destruction.

In 2003, Shao et al. [20] induced silk fiber by UV/ozone irradiation and elucidated the structural changes by means of FT-IR spectroscopy.

1.5 The objectives of this research

The objectives of this research are to simplify the preparation of silk fibroin nanoparticles from silk fiber by precipitation method and to characterize the molecular characteristics of silk fibroin nanoparticles by means of ATR FT-IR microspectroscopy.

1.6 The scopes of this research

1. To prepare silk fibroin nanoparticles from silk fiber by precipitation method.
2. To study the molecular characteristics of silk fibroin nanoparticles by means of ATR FT-IR microspectroscopy.
3. To study the morphology of silk fibroin nanoparticles by means of scanning electron microscopy.
4. To study the deposition of silver nanoparticles on silk fibroin nanoparticles by means of UV-Visible spectroscopy and transmission electron microscopy.



ศูนย์วิจัยทรัพยากร
จุฬาลงกรณ์มหาวิทยาลัย

CHAPTER II

THEORETICAL BACKGROUND

2.1 Fundamentals of spectroscopy

Infrared spectroscopy is the study of the interaction of infrared radiation with a chemical substance. Light is an electromagnetic wave. It composes of electric wave (electric vector (E)) and magnetic wave (magnetic vector (H)). The electric wave and magnetic wave are perpendicular to each other and to the direction of propagation as shown in Figure 2.1 [21].

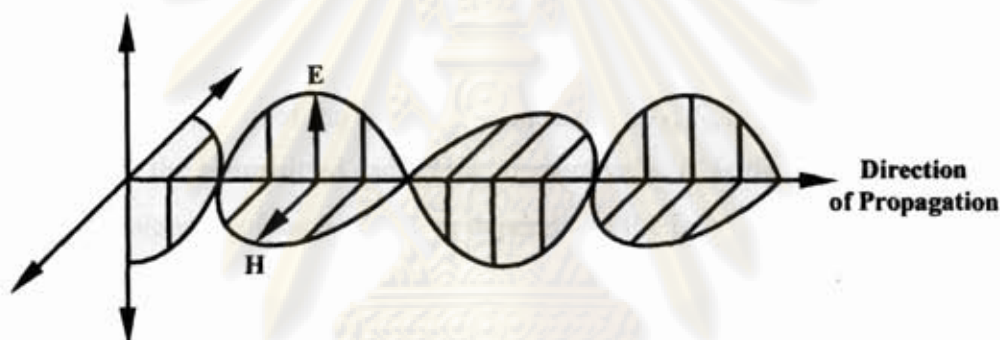


Figure 2.1 Propagation of a linearly polarized electromagnetic wave in the direction of propagation. Electric (E) and magnetic (H) vectors are always perpendicular to each other and to the direction of propagation.

Infrared spectroscopy gives spectral information of molecular structure and chemical composition. It measures the infrared intensity versus wavenumber. When infrared radiation passes through a sample, the frequencies of infrared radiation are absorbed by chemical functional group of a sample in specific wavenumber and leading the chemical bonds in molecule to vibrate. The position of wavenumber and chemical structure are related to chemical functional group in a sample.

When electromagnetic radiation impinges on the matter, radiation of the incident beam can be reflected, scattered, transmitted or absorbed by a sample depending on the experimental situation. A schematic illustration for an interaction between light and matter is illustrated in Figure 2.2 [21].

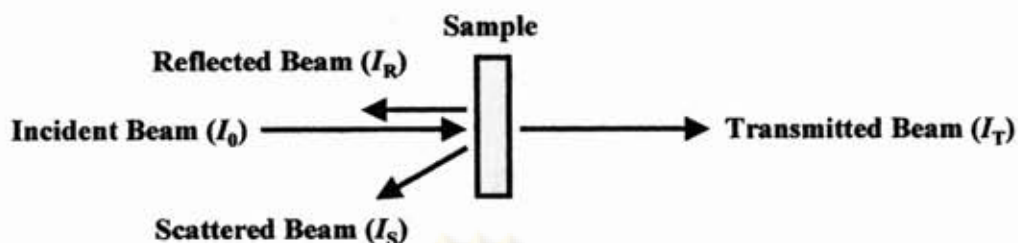


Figure 2.2 Interactions of light with matter.

The total amount of incident energy is the sum of reflected, scattered, transmitted, and absorbed light. This process can be expressed by the following relationship [21]:

$$I_0 = I_R + I_S + I_T + I_A \quad (2.1)$$

where I_0 is the intensity of the incident radiation and I_R , I_S , and I_T are the reflected, the scattered, and the transmitted radiations, respectively. I_A is the radiation absorbed by matter. The intensity of each radiation depends on the intensity and wavelength of the incident radiation, the optical properties of the specimen, the concentrations of species, and the geometry of the experimental setup.

Considering electromagnetic radiation impinges on a sample, a fraction of the incident radiation was absorbed by a sample. In order to measure the region and amount of light being absorbed by a sample, it is necessary to measure the ratio of transmitted intensities (I_T) and incident intensities (I_0) of radiation. The transmittance of a sample is obtained from these ratios. This relationship can be quantitatively related to the chemical composition of a sample by the *Beer-Lambert law* as [16]:

$$\frac{I}{I_0} = e^{-A(\bar{\nu})} = e^{-c_2 \epsilon(\bar{\nu})l} \quad (2.2)$$

where $A(\bar{\nu})$ is the absorbance of a sample at a given wavenumber $\bar{\nu}$, c_2 is the concentration of the absorbing functional group, $\epsilon(\bar{\nu})$ is the wavenumber-dependent absorption coefficient, and l is the film thickness for the infrared beam at a normal incidence to the sample surface.

2.2 Attenuated Total Reflection Fourier Transform Infrared (ATR FT- IR) Spectroscopy

Attenuated Total Reflection Fourier Transform Infrared Spectroscopy is used for analysis of surface of materials and is a non-destructive technique. It is a method of internal reflection, which requires a medium called internal reflection element (IRE) or the *ATR crystal*. The infrared radiation is directed into IRE, which high refractive index with an angle that total internal reflections occur inside IRE. The light exits IRE and passes through the spectrometer to the detector. At each reflection a part of the light called the *evanescent wave* passes IRE interface and interacts with a sample place in close contact with IRE. The infrared spectrum may be collected. The surface of a sample is pressed into optical contact of IRE such as zinc selenide (ZnSe), germanium (Ge), and diamond. The materials of IRE have an effect on the ATR measurement because materials of different refractive index affect the depth of penetration and the occurrence of anomalous dispersion [22].

When the electromagnetic radiation traveling within IRE made of a high refractive index material impinges on the interface with a lower refractive material, the angle of incidence larger than the critical angle. This critical angle (θ_c) is relative to the refractive index as shown in equation 2.3 [23].

$$\theta_c = \sin^{-1}(n_2 / n_1). \quad (2.3)$$

where n_2 is the refractive index of a sample and n_1 is the refractive index of IRE.

In ATR experiment, IRE is contacted with a sample as shown in Figure 2.3. IRE is the infrared transparent material and has a refractive index n_1 . A sample is infrared absorbing material and has a complex refractive index at frequency ν can be expressed by equation 2.4.

$$\hat{n}_2(\nu) = n_2(\nu) + ik_2(\nu) \quad (2.4)$$

where n_2 and $k_2(\nu)$ are the refractive index and absorption index of a sample, respectively.

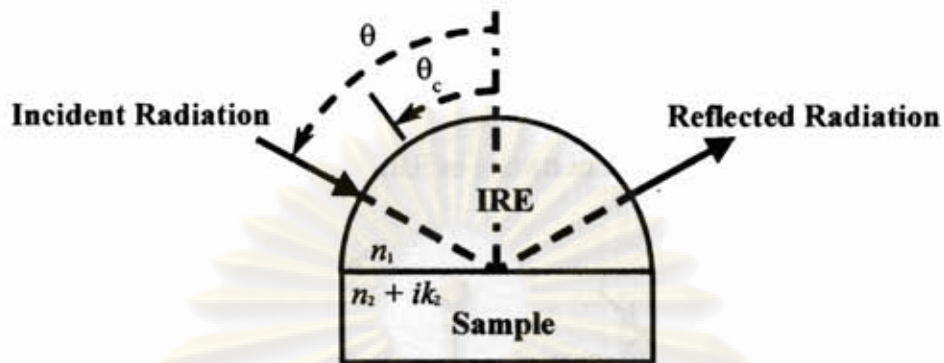


Figure 2.3 Ray tracing under total internal reflection.

2.2.1 Principle of light reflection and refraction

Refraction and reflection occur, when the electromagnetic radiation passes from one medium to a sample, which different refractive index that has a difference in propagation velocity through two media. If light propagates through an incident medium with refractive index n_1 and enters a medium with refractive index n_2 (Figure 2.5), the light path will be changed and the extent of refraction is given by the following relationship known as Snell's law [21].

$$n_1 \sin \alpha_1 = n_2 \sin \alpha_2 \quad (2.5)$$

where α_1 and α_2 are the angles of incidence and refraction, respectively.

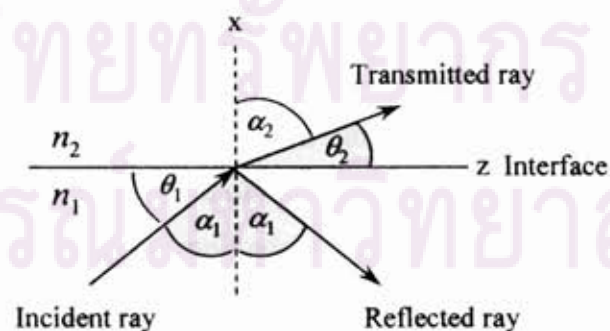


Figure 2.4 Reflection and refraction of a plane wave at a dielectric interface based on Snell's law.

2.2.2 Internal Reflection Element (IRE)

Internal reflection element (IRE) or the ATR crystal is a material of high refractive index and is transparent throughout the mid-infrared region. IRE can divide into two main types: single reflection type with a hemispherical IRE and multiple reflection type with a trapezoidal IRE as shown in Figure 2.5.

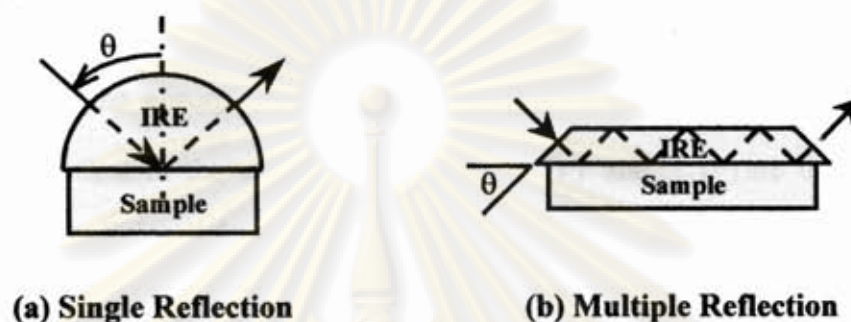


Figure 2.5 IRE configurations commonly used in ATR experimental setups: (a) Single reflection variable-angle hemispherical crystal and (b) Multiple reflection single-pass crystal.

2.2.3 ATR spectral intensity and penetration depth

ATR FT-IR spectroscopy is a surface analysis technique. This technique based on infrared radiation. In ATR configuration, the IRE is the infrared transparent material. On the other hand, a sample is the infrared absorbing material and has a complex refractive index at frequency ν of $\hat{n}_2(\nu) = n_2(\nu) + ik_2(\nu)$. When electromagnetic radiation traveling within IRE impinges at the surface of a sample of lower refractive index at an angle of incidence greater than the critical angle, the evanescent field is generated at the IRE/sample interface. A sample is absorbing at the coupled frequency. The intensity of the reflected radiation becomes smaller than that of the incident radiation. The magnitude of the reflection loss is proportional to the product between the evanescent field amplitude and the imaginary part of the complex dielectric constant. The absorptance in the ATR configuration is related to reflectance as shown in equation [24].

$$A(\theta, \nu) = 1 - R(\theta, \nu) \quad (2.6)$$

where $A(\theta, \nu)$ and $R(\theta, \nu)$ are the absorptance and reflectance, respectively. In general, ATR absorptance can be expressed in terms of experimental conditions and material characteristic as shown in equation [25].

$$A(\theta, \nu) = \frac{4\pi\nu}{n_1 \cos\theta} \int_0^\infty n_2(\nu)k_2(\nu) \langle E_z^2(\theta, \nu) \rangle dz \quad (2.7)$$

where $A(\theta, \nu)$ is the absorptance, $\langle E_z^2(\theta, \nu) \rangle$ is the *mean square evanescent field* (MSEvF) at depth z in the absorbing medium, $n_2(\nu)$ and $k_2(\nu)$ are the refractive index and the absorption index of a sample, and n_1 is the refractive index of the IRE.

The penetration depth is the distance from the interface of materials where the evanescent field strength decays to $1/e$ (roughly 13%) of its value at the interface. The penetration depth is given by the following equation [26]:

$$d_p = \frac{1}{2\pi\nu n_1 (\sin^2\theta - (n_2/n_1)^2)^{1/2}} \quad (2.8)$$

where θ is the angle of incidence, ν is the frequency of the infrared radiation and n_1 , n_2 are the refractive index of the IRE and a sample.

ศูนย์วิทยทรัพยากร
จุฬาลงกรณ์มหาวิทยาลัย

CHAPTER III

EXPERIMENTAL SECTION

The general, silk fibroin nanoparticles were prepared by pulverizing natural silk fibers with pulverizer or spray-drying silk fibroin solution with spray-dryer. In this study, silk fibroin nanoparticles were prepared by precipitation of silk fibroin solution in organic solvents. The molecular conformation of the silk fibroin fiber and silk fibroin nanoparticles were studied by ATR FT-IR microspectroscopy. Particles size and morphology of silk fibroin nanoparticles were analyzed by scanning electron microscope (SEM). This chapter is divided into three sections: preparation methods of the silk fibroin nanoparticles, characterization of silk fibroin nanoparticles, and the application of silk fibroin nanoparticles as a substrate for silver nanoparticles. The silver nanoparticles deposited silk fibroin nanoparticles were analyzed by UV-Visible spectrometer and transmission electron microscope (TEM).

3.1 Materials

1. Degummed *Bombyx mori* silk fibers from Queen Sirikit Sericulture Regional Office (Northern Part: Phrae Province)
2. Lithium bromide (LiBr) was purchased from Sigma-Aldrich Laborchemikalien GmbH, Thailand.
3. Sodium chloride (NaCl) was purchased from Merck KGaA, Thailand.
4. Organic solvents (methanol, ethanol, and *iso*-propanol) were purchased from Merck KGaA, Thailand.
5. Deionized water
6. Silver nanoparticles were freshly prepared by Sensor Research Unit (Department of Chemistry, Faculty of Science, Chulalongkorn University, Thailand) at the concentrations of 50, 100, and 200 ppm.

3.2 Experimental section

3.2.1 Preparation of *Bombyx mori* silk fibroin solution

The degummed silk fiber, which were degummed by 0.02 M Na_2CO_3 solution was dissolved in aqueous solution of 9.3 M LiBr (5% w/v) for 6 h at 40-60 °C. This solution was filtered by a filter paper (Whatman® Schleicher & Schuell, No.1) to remove a small amount of insoluble silk. The solution, then, was dialyzed in deionized water by dialysis tubing cellulose membrane (MWCO 12,400) for 3 days at room temperature for removing salts (LiBr). The final concentration of the silk fibroin solution was approximately 1.5% w/v. This concentration was calculated by weighting the residual solid of solution after drying at 60 °C.

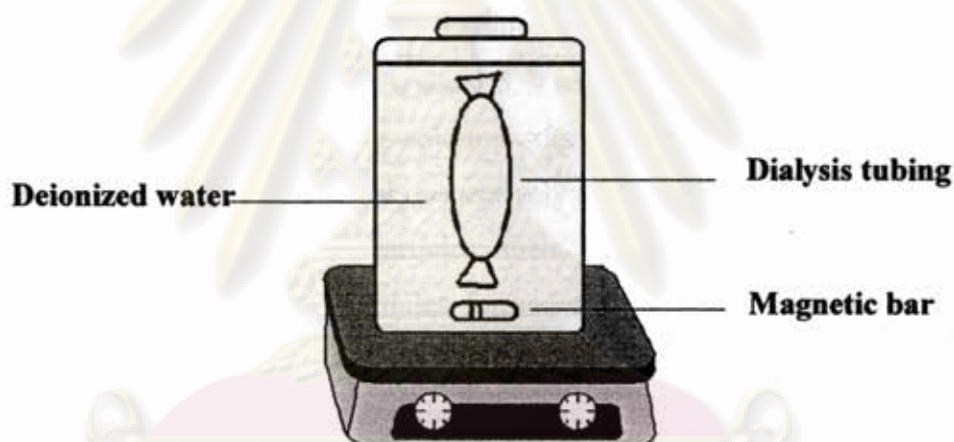


Figure 3.1 The dialysis tubing of silk fibroin solution.

3.2.2 Preparation of the silk fibroin films

The silk fibroin solution was dropped onto a glass slide plate as the substrate at room temperature and then dried at 60 °C. After that the molecular conformation of silk fibroin films was analyzed by ATR FT-IR microspectroscopy.

3.2.3 Preparation of the precipitating solution

The solution for precipitation of silk fibroin nanoparticles is called the precipitating solution. The precipitating solution was prepared by adding the aqueous

solution of 0.5 M NaCl into silk fibroin solution. To study the effect of the concentration of NaCl, we varied the final concentration of NaCl in silk fibroin solution as follows: 0.00 M, 0.015 M, 0.05 M, and 0.25 M. 10 mL of each concentration of the precipitating solution was dropped in 50 mL of methanol. The silk fibroin nanoparticles, then, formed and suspended in methanol. Particles size and morphology of these nanoparticles were characterized by SEM. The suitable concentration of NaCl was also used in the next procedure to prepare silk fibroin nanoparticles.

3.2.4 Preparation of silk fibroin nanoparticles

Silk fibroin nanoparticles were prepared by precipitation of the suitable precipitating solution in organic solvents. To study the effect of the concentration of the precipitating solution, we varied the volume ratio of the precipitating solution per organic solvents as follows: 1:1, 1:3, and 1:5. 9 sets of the preparations obtained were tested. 10 mL of the precipitating solution was dropped in 50, 30, and 10 mL of methanol, ethanol, and *iso*-propanol, respectively at room temperature with stirring all the time. The silk fibroin nanoparticles, then, formed and suspended in organic solvents, the silk fibroin nanoparticles formed and suspended in organic solvents. Particles size and morphology of these nanoparticles were characterized by SEM. The molecular conformation of silk fibroin films was analyzed by ATR FT-IR microspectroscopy.

3.2.5 The deposition of silver nanoparticles on silk fibroin nanoparticles

Silk fibroin nanoparticles suspended in methanol were washed five times with deionized water to eliminate the organic solvent. 50, 100, and 200 ppm silver nanoparticles colloidal solution were measured by UV-Visible spectrometer. 10 mL of these were added into 5 mL of silk fibroin nanoparticles suspension (with silk fibroin weight about 0.055 ± 0.010 g). The mixture was shaken until the homogeneous phase was attained and allowed to settle overnight at room temperature, then silk fibroin nanoparticles were precipitated again. The concentrations of silver nanoparticles in supernatant were measured by UV-Visible spectrometer. Before collecting spectrum, the sample was twenty times diluted with deionized water. The

molecular conformation of silk fibroin nanoparticles was analyzed by ATR FT-IR microspectroscope. The morphology of silver nanoparticles deposited on silk fibroin nanoparticles was characterized by TEM.

The release of silver nanoparticles was tested by adding 20 mL of the deionized water into 0.055 ± 0.010 g of silver-deposited silk fibroin nanoparticles of 50 ppm, 100 ppm, and 200 ppm, respectively. The mixture was shaken until the homogeneous phase was attained and allowed to settle overnight at room temperature, then silk fibroin nanoparticles were precipitated again. The concentrations of silver nanoparticles in supernatant were measured by UV-Visible spectrometer.

3.3 Characterization of silk fibroin nanoparticles

3.3.1 ATR FT-IR microspectroscopy

Molecular conformation of silk fibroin nanoparticles was acquired by the Germanium (Ge) μ IRE. All ATR spectra were collected by a ContinuumTM infrared microscope equipped with a mercury-cadmium-tellurium (MCT) detector that attached to the Nicolet 6700 FT-IR Spectrometer. Ge μ IRE was placed on the objective microscope and the silk fibroin was placed on a glass slide and positioned on the microscope stage. For spectral acquisition of samples, the stage of microscope was raised in order to bring sample contact a Ge μ IRE. The ATR spectra of samples were acquired in the reflection mode of infrared microscope. The information of secondary structure of silk fibroin nanoparticles was acquired by curve fitting analysis. The Amide I region between $1740-1580\text{ cm}^{-1}$ was fitted with Gaussian and Lorentzian functions. The peak position and peak area of the fitted peak were identified and estimated to show the secondary structure information. The second-derivative spectra were used as a parameter for curve fitting analysis in Amide I region.

3.3.1.1 Instrument

1. Nicolet 6700 FT-IR spectrometer equipped with a mercury cadmium-telluride (MCT) detector.
2. Continuum™ infrared microscope with 15X Cassegrain infrared objective and 10X glass objective.
3. Homemade slide-on Ge μ IRE

3.3.1.2 Default Spectral Acquisition Parameter

Nicolet 6700 FT-IR Spectrometer

Instrumental Setup

Source	Standard Global™ Infrared Light Source
Detector	MCT
Beam splitter	Ge-coated KBr

Acquisition Parameters

Spectral resolution	4 cm^{-1}
Number of scans	128 scans
Spectral format	Absorbance
Mid-infrared range	4000-650 cm^{-1}

Advanced Parameters

Zero filing	none
Apodization	Happ-Genzel
Phase correction	Mertz

Continuum™ Infrared Microscope

Instrumental Setup

Detector	MCT
Objective	15X Schwarzschild-Cassegrain
Aperture size	150 μm x 150 μm



Figure 3.2 ATR FT-IR microscope: (A) Continuum™ infrared microscope attached to the Nicolet 6700 FT-IR spectrometer, (B) the slide-on Ge μ IRE is fixed on the position of slide-on housing on the infrared objective, and (C) Homemade slide-on Ge μ IRE.

3.3.2 Scanning electron microscopy

Particles size and morphology were characterized by SEM of JSM-6480LV model at 15 kV of acceleration voltage as shown in Figure 3.3. For capturing the image of samples, the colloidal solution containing nanoparticles was dried on a glass slide. Samples were then sputter-coated by gold films. The samples were moved to specimen chamber and then particles size and morphology of samples were analyzed.

ศูนย์วิจัยทรัพยากร
จุฬาลงกรณ์มหาวิทยาลัย



Figure 3.3 JEOL JSM-6480LV analytical scanning electron microscope.

3.3.3 Transmission electron microscopy

Particles size and morphology of silver nanoparticles deposited on silk fibroin nanoparticles were characterized by TEM zero A H-7650 model at 100 kV of acceleration voltage as shown in Figure 3.4. For capturing the images of samples, samples were prepared by placing a drop of solution sample on a Formvar films on copper grids. The samples were moved to specimen chamber and then the morphology of samples was analyzed.



Figure 3.4 Hitachi zero A H-7650 analytical transmission electron microscope.

3.3.4 UV-Visible spectroscopy

The deposition of silver nanoparticles on silk fibroin nanoparticles was analyzed by UV-Visible spectrometer ocean optics portable model as shown in Figure 3.5.

Instrumental Setup

Model	USB4000
Source	Deuterium-Halogen light source DH 2000
Wavelength range	UV-Vis-NIR
Detector	Toshiba TCD1304AP, 3648-element linear silicon CCD array
Grating	600 Line Blazed at 300 nm
Bandwidth	200-1100 nm

Spectral Acquisition Parameter

Software	Ocean Optics Inc. Spectra Suit
Integration time	10 milliseconds
Scans to Average	128 scans
Box car width	10 nm
Spectral format	Absorbance
Spectra range	250-800 nm

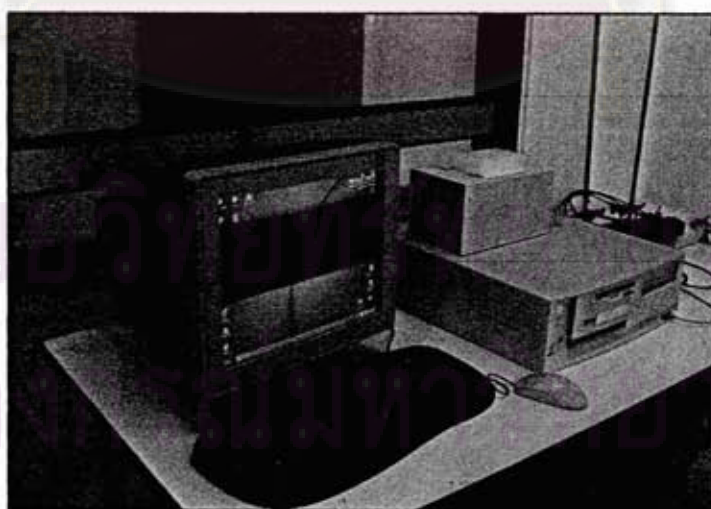


Figure 3.5 Toshiba USB4000 ocean optics portable UV-Visible spectrometer.

The silver nanoparticles colloidal solutions of 50, 100, and 200 ppm were twenty times dilution with deionized water. The last concentrations were 2.5, 5, and 10 ppm, respectively. The supernatant was twenty times diluted with deionized water. After that UV spectra of the diluted silver nanoparticles colloidal solution and the supernatant were collected. Before collecting spectra, the deionized water spectrum was collected as blank sample.



ศูนย์วิจัยทรัพยากร
จุฬาลงกรณ์มหาวิทยาลัย

CHAPTER IV

RESULTS AND DISCUSSION

Silk fibroin nanoparticles were prepared by precipitation of silk fibroin solution in methanol, ethanol, and *iso*-propanol. In this case, it is necessary to study the effects of the concentration of NaCl and the precipitating solution. After that, the molecular conformation of silk fibroin will be elucidated by ATR FT-IR microspectroscopy. Particles size and morphology of silk fibroin nanoparticles will also be investigated by SEM. The last section of the results and discussion will show the application of silk fibroin nanoparticles for supporter of silver nanoparticles.

4.1 The effect of NaCl in silk fibroin solution for precipitation in methanol

The aqueous solution of 0.5 M NaCl was added into silk fibroin solution by varying the final concentration of NaCl as follows: 0.00 M, 0.015 M, 0.05 M, and 0.25 M. After that, the solution was precipitated in methanol. The obtained silk fibroin nanoparticles suspended in methanol. Particles size and morphology of silk fibroin nanoparticles were characterized by SEM.

Figure 4.1 shows SEM images of silk fibroin nanoparticles. It was found that at 0.00 M and 0.015 M of NaCl solution; silk fibroin solution did not precipitate to particles as shown in Figure 4.1 (a and b), respectively. At 0.05 M and 0.25 M of NaCl solution, silk fibroin solution precipitated to particles as shown in Figure 4.1 (c and d), respectively. At the higher NaCl concentration, the number of sodium ions and chloride ions were increased. The ions are solvated by water molecules—they are hydrated ions. Therefore, the water was easily removed from silk fibroin molecules when the concentration of NaCl increased [27-28]. At the lower NaCl concentration, the water molecules still remained in silk fibroin molecule. Therefore, silk fibroin solution did not precipitate to particles. At 0.25 M of NaCl solution, some the small particles were aggregated to bigger particles as shown in Figure 4.1(d). The particles size of silk fibroin particles at different final concentration of NaCl as shown in Table 4.1. The optimum of final concentration of NaCl in silk fibroin solution for

precipitation in methanol was 0.05 M, which had the small particles sizes and the particles did not aggregate.

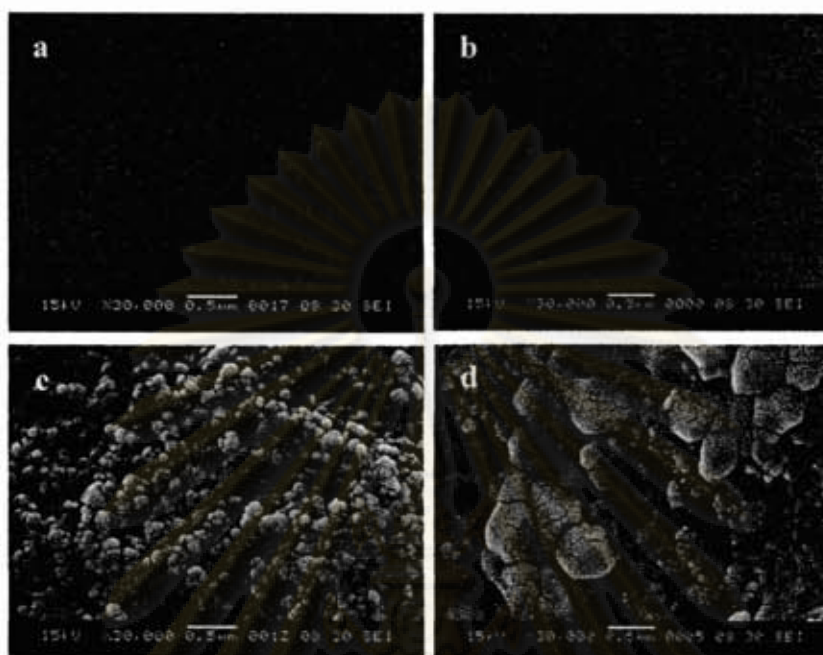


Figure 4.1 SEM images of silk fibroin particles at different concentrations of NaCl: (a) 0 M, (b) 0.015 M, (c) 0.05 M, and (d) 0.25 M.

Table 4.1 The particles size of silk fibroin particles at different concentration of NaCl.

Final concentration (M) of NaCl in precipitated solution	Particles size (nm)
0	-*
0.015	-*
0.05	98.40 ± 2.90
0.25	276.71 ± 0.03

* No precipitation

4.2 The effect of silk fibroin concentration on precipitation in organic solvents

To study the effect of the concentration of the precipitating solution, the volume ratios of the precipitating solution per organic solvents (methanol, ethanol, and *iso*-propanol) were varied as follows: 1:5, 1:3, and 1:1 (16.6%, 25%, and, 50% v/v, respectively). A total of nine sets of the preparations were tested. A 10 mL of the precipitating solution was dropped into 50, 30, and 10 mL of methanol, ethanol, and *iso*-propanol, respectively at room temperature with vigorous stirring. Silk fibroin nanoparticles formed and suspended in organic solvents. Particles size and morphology were characterized by SEM.

Table 4.2 The particles size of silk fibroin particles at different silk fibroin concentrations.

Concentration of silk fibroin solution (% v/v)	Particles size (nm)		
	Precipitated in Methanol	Precipitated in Ethanol	Precipitated in <i>iso</i> -Propanol
16.6	98.43 ± 2.92	92.73 ± 3.83	98.60 ± 2.48
25	162.10 ± 6.30	111.84 ± 4.90	139.69 ± 6.62
50	~1000	~1000	~1000

Table 4.2 shows the size of the silk fibroin particles obtained from precipitation of silk fibroin solution in methanol, ethanol, and *iso*-propanol. For all organic solvents, it was found that the particles size decreased with the decreasing silk fibroin concentrations. At higher silk fibroin concentration, the particles aggregated. The morphology of silk fibroin particles was different depending on the silk fibroin concentration as shown in Figure 4.2 and their corresponding photographs shown in Figure 4.3. According to the morphology, the volume of silk fibroin solution should not be greater than 16.6% v/v because the more silk fibroin concentration was, more particles aggregated.

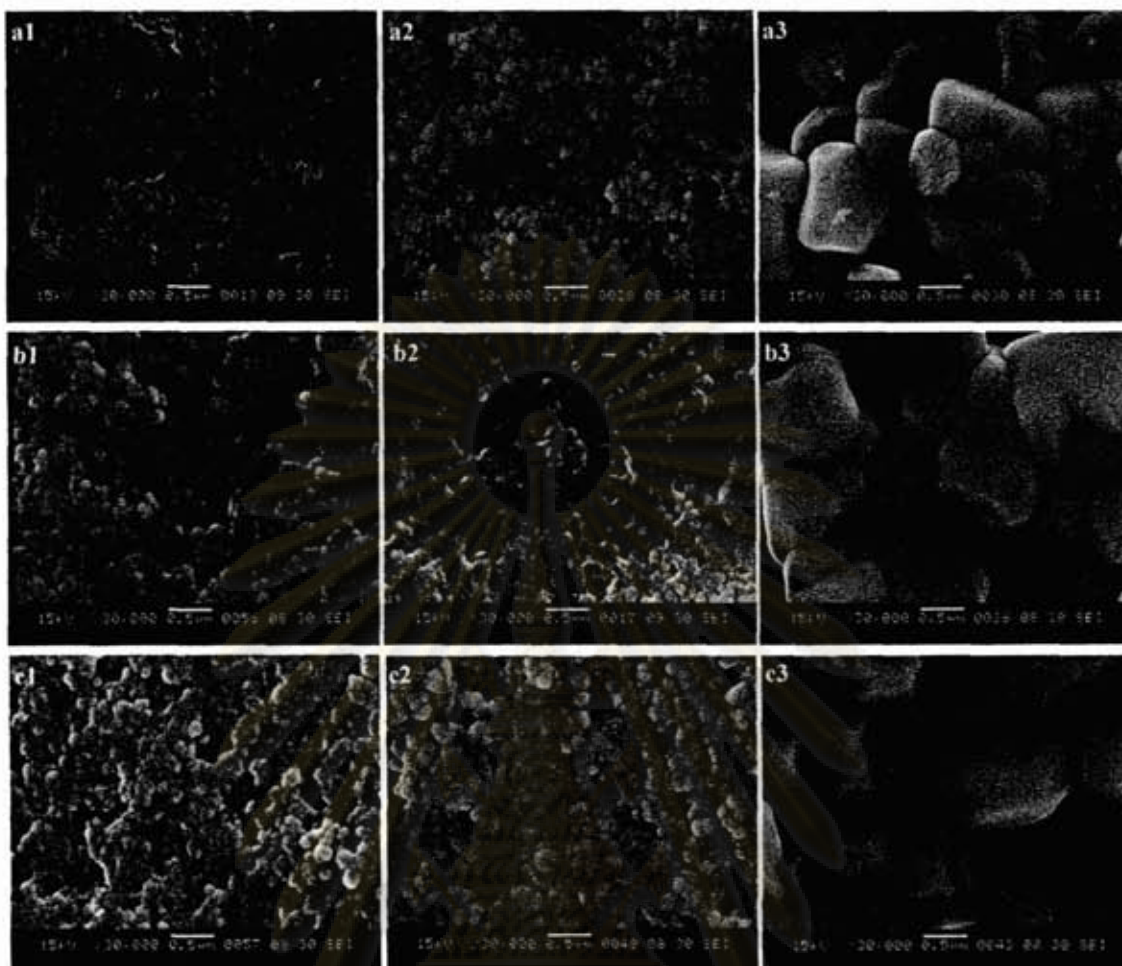
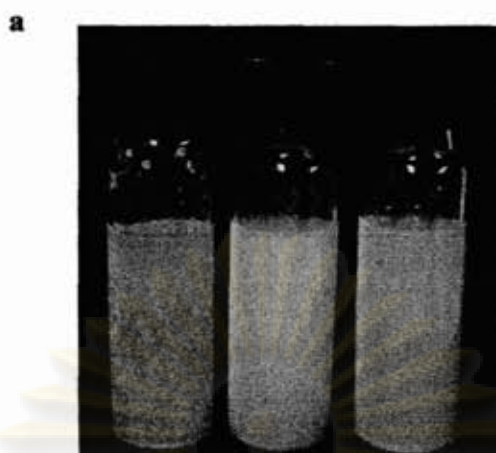


Figure 4.2 SEM images of silk fibroin particles at different silk fibroin concentrations: (a1) 16.6%, (a2) 25%, (a3) 50% v/v. Silk fibroin solutions were precipitated in methanol, (b1) 16.6%, (b2) 25%, (b3) 50% v/v. Silk fibroin solutions were precipitated in ethanol, (c1) 16.6%, (c2) 25%, (c3) 50% v/v. Silk fibroin solutions were precipitated in *iso*-propanol.

ศูนย์วิทยทรัพยากร
จุฬาลงกรณ์มหาวิทยาลัย



50% v/v 25% v/v 16.6% v/v



50% v/v 25% v/v 16.6% v/v



50% v/v 25% v/v 16.6% v/v

Figure 4.3 Photograph of silk fibroin particles at different silk fibroin concentrations: (a) silk fibroin particles precipitated in methanol, (b) silk fibroin particles precipitated in ethanol, and (c) silk fibroin particles precipitated in *iso*-propanol.

SEM images of silk fibroin nanoparticles shown in Figure 4.2 indicated that the particles sizes were increased with increasing the concentrations of silk fibroin solution. The optimum volume ratio of the silk fibroin solution per organic solvents was 16.6% v/v, because it contained the smallest particles sizes. The yield of silk fibroin nanoparticles was calculated as follows:

$$\% \text{ yield} = \frac{\text{weight of silk fibroin nanoparticles (g)} \times 100}{\text{weight of silk fibroin fiber (g)}} \quad (4.1)$$

For example;

Silk fibroin concentration of 1.5% w/v was used in order to precipitate silk fibroin nanoparticles in methanol. Silk fibroin nanoparticles were dried by vacuum dry and the mass of silk fibroin nanoparticles was measured.

No. # 1

Weight of silk fibroin fiber = 1.974 g

Weight of silk fibroin nanoparticles = 1.532 g

$$\begin{aligned} \% \text{ yield} &= \frac{1.532 \times 100}{1.974} \\ &= 77.6 \end{aligned}$$

No. # 2

Weight of silk fibroin fiber = 4.030 g

Weight of silk fibroin nanoparticles = 4.950 g

$$\begin{aligned} \% \text{ yield} &= \frac{4.950 \times 100}{4.030} \\ &= 81.41 \end{aligned}$$

Average yield = 79.48%

The average yield of silk fibroin nanoparticles precipitated in methanol, ethanol and *iso*-propanol were 79.48, 78.56, and 73.94%, respectively.

4.3 Chemical information of silk fibroin

The silk fibroin protein consists of more than 16 amino acids. The silk fibroin is mainly composed of non-polar amino acids (glycine and alanine). The ATR FT-IR

technique for the molecular characterization of silk fibroin. The application of the slide-on Ge μ IRE for a single silk fibroin fiber and silk fibroin nanoparticles were demonstrated and the results were shown in Figure 4.4-4.8.

4.3.1 Chemical information of silk fibroin fiber

Silk fibroin fiber was analyzed by ATR FT-IR microspectroscopy with the homemade slide-on Ge μ IRE. The ATR FT-IR spectra of single silk fibroin fiber are shown in Figure 4.4. A sharp band centered at 3282 cm^{-1} is N-H stretching vibration. The absorption bands at 1624 , 1514 , and 1230 cm^{-1} are associated with Amide I, Amide II, and Amide III vibrations, respectively. The absorption bands of Amide I vibration mode consist of two components including the C=O stretching vibration and small contribution from N-H scissoring vibration. The absorption bands of Amide II vibration mode consist of two components including the N-H wagging vibration and C-N stretching vibration. The absorption bands of Amide III vibration mode consist of two components including the N-H twisting vibration plus C-N stretching vibration and the contribution from O=C-N bending vibration.

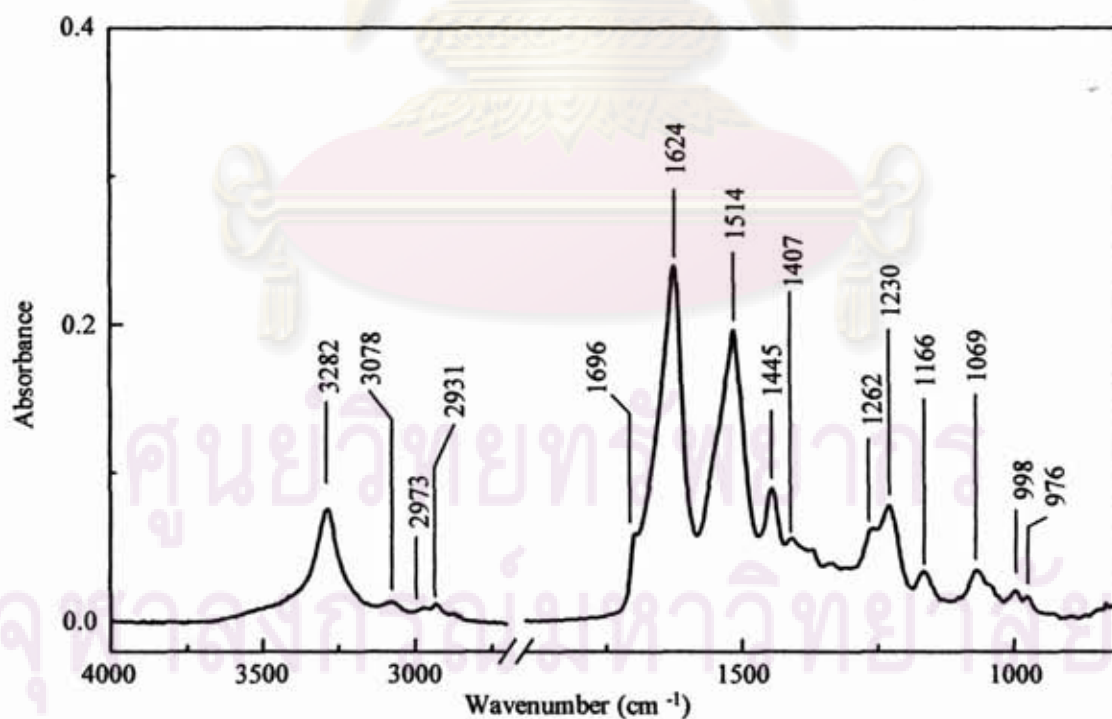


Figure 4.4 ATR FT-IR spectrum of single silk fibroin fiber acquired by the slide-on Ge μ IRE.

The absorption bands centered at 2973 and 2931 cm^{-1} are the C-H stretching vibrations while the bands centered at 1445 and 1407 cm^{-1} are the C-H deformation vibrations. The weak band at 1696 cm^{-1} is assigned to be the antiparallel β -sheet structure [24]. The absorption bands at 998 and 976 cm^{-1} attributed to the Gly-Ala sequences, respectively. The IR peak assignments are summarized in Table 4.3.

Table 4.3 Peak assignments of single silk fibroin fiber [18, 29-37].

Wavenumber (cm^{-1})	Current work	Peak Assignments
3385-3160	3282	Symmetric N-H stretching
3100-3070 (w)	3078	Overtone of Amide II
2975-2950 (m, s)	2973	Asymmetric C-H stretching of CH_3
2940-2915 (m, s)	2931	Asymmetric C-H stretching of CH_2
1698-1690 (w)	1696	Antiparallel β -sheet
1695-1610 (s)	1624	<u>Amide I</u> C=O stretching and a small contribution from N-H bending (scissoring)
1575-1480 (s)	1514	<u>Amide II</u> N-H bending (wagging) plus C-N stretching
1480-1440 (m)	1445	C-H bending (scissoring) of CH_2
1410-1350 (m, s)	1407	C-H bending (wagging) of CH_3
1305-1200 (w, m)	1262, 1230	<u>Amide III</u> N-H bending (twisting) plus C-N stretching and the contribution from O=C-N bending
1175-1165 (s)	1166	O-H bending of phenolic residue in Tyr
1100-1050 (m)	1069	C-N stretching of $\text{RCH}_2\text{-NH}_2$, $\text{R}_2\text{CH-NH}_2$
1060-900 (w, m)	998, 976	C-C skeletal of Gly-Ala sequences

The first- and the second-derivative spectra of silk fibroin fiber are shown in Figure 4.5. The first- and the second-derivative spectra show distinct weak bands at 1696, 998 and 976 cm^{-1} of both the first- and the second-derivative spectra. The weak band at 1696 cm^{-1} is assigned to be the antiparallel β -sheet structure and the weak

bands at 998 and 976 cm^{-1} are assigned to be Gly-Ala sequences, which are the character of silk fibroin.

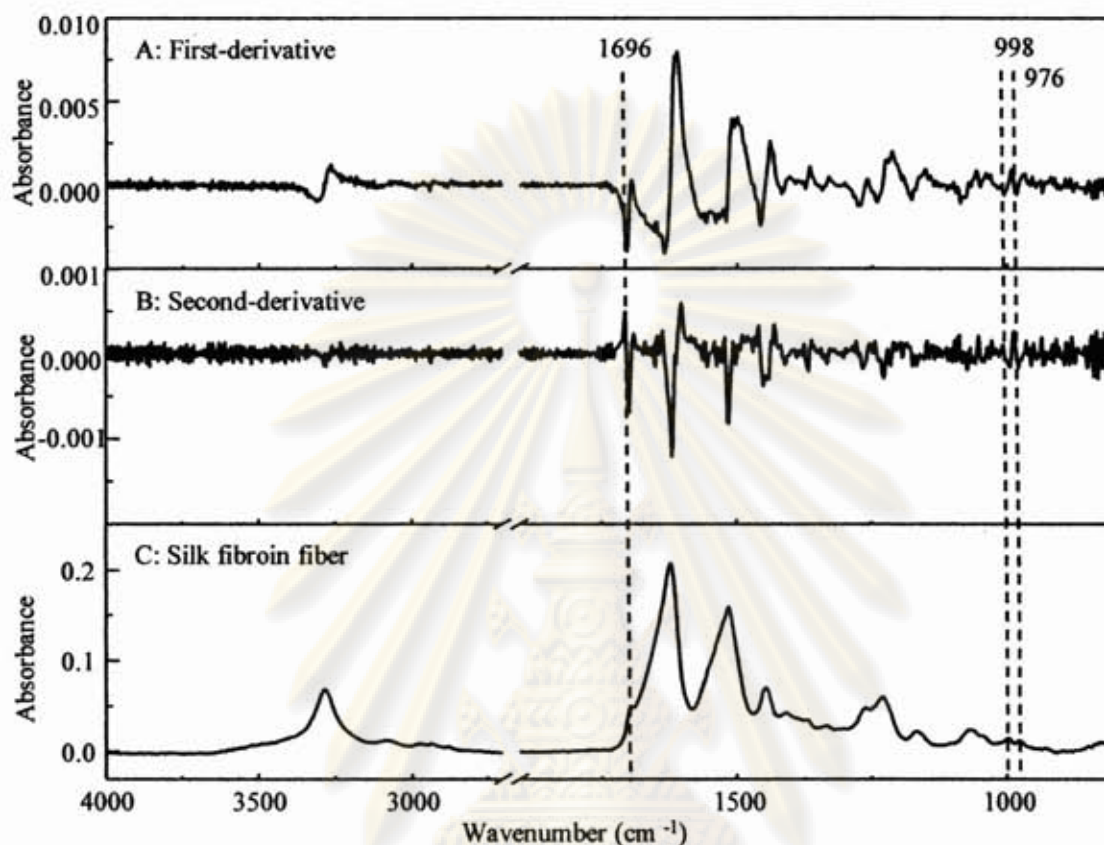


Figure 4.5 Derivative spectra of single silk fibroin fiber: (A) first-derivative and (B) second-derivative.

4.3.2 Chemical information of silk fibroin nanoparticles precipitated in organic solvents

The ATR FT-IR spectra of silk fibroin nanoparticles precipitated in methanol, ethanol, and *iso*-propanol are shown in Figures 4.6, 4.7, and 4.8, respectively. The IR peak assignments of silk fibroin nanoparticles precipitated in methanol, ethanol, and *iso*-propanol are summarized in Table 4.4.

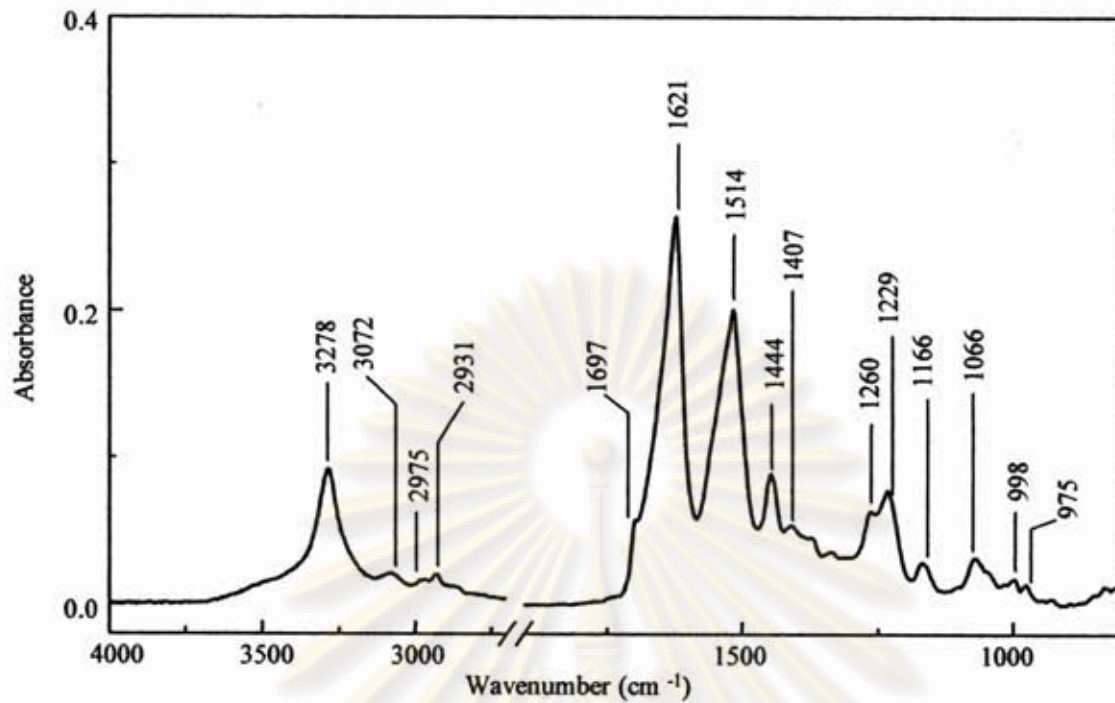


Figure 4.6 ATR FT-IR spectrum of silk fibroin nanoparticles precipitated in methanol by the slide-on Ge μ IRE.

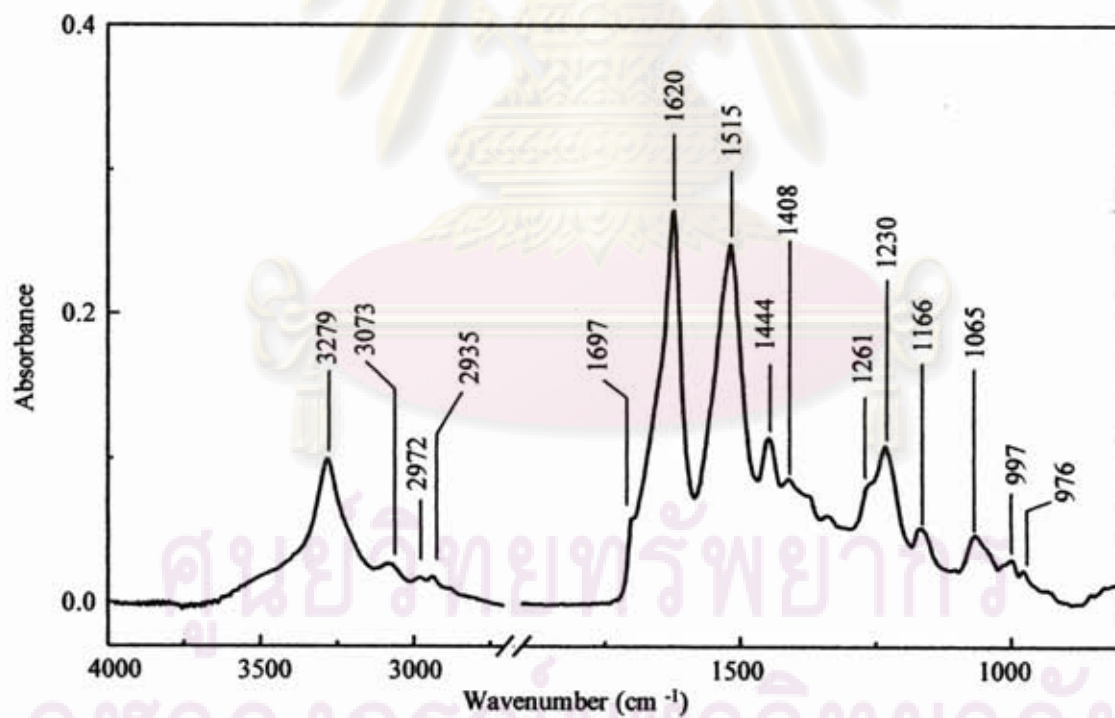


Figure 4.7 ATR FT-IR spectrum of silk fibroin nanoparticles precipitated in ethanol by the slide-on Ge μ IRE.

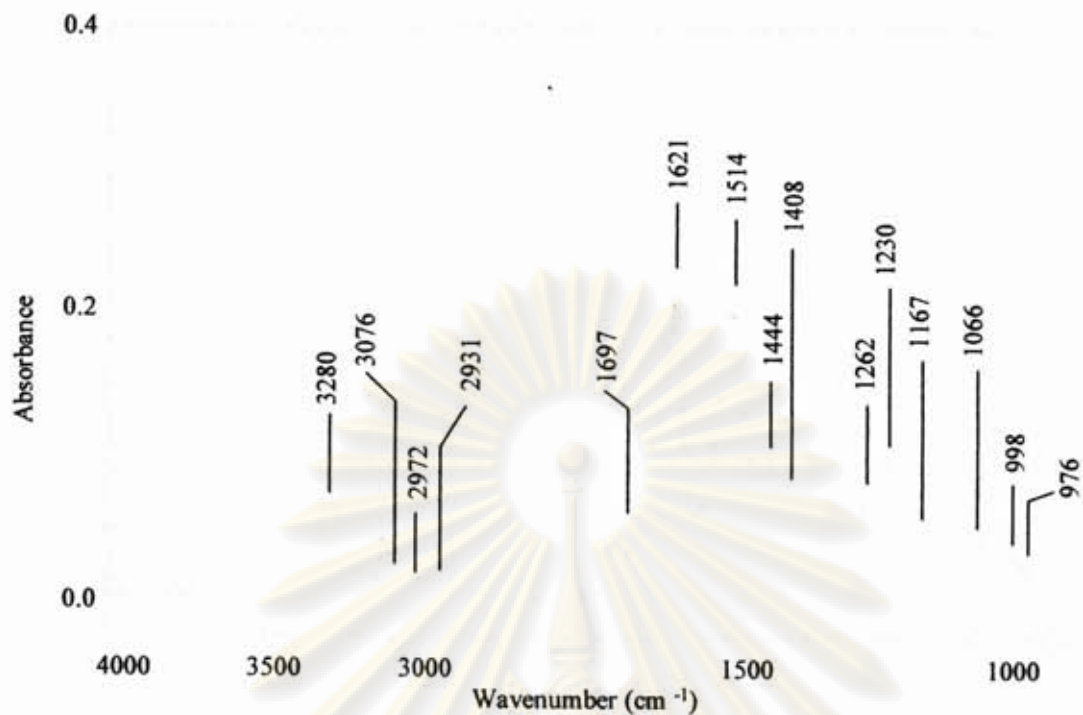


Figure 4.8 ATR FT-IR spectrum of silk fibroin nanoparticles precipitated in *iso*-propanol by the slide-on Ge μ IRE.

Table 4.4 Peak assignments of silk fibroin nanoparticles [18, 29-37].

Wavenumber (cm^{-1})	Current Work			Peak Assignments
	Methanol	Ethanol	<i>iso</i> - Propanol	
3385-3160	3278	3279	3280	Symmetric N-H stretching
3100-3070	3072	3073	3076	Overtone of Amide II
2975-2950	2975	2972	2972	Asymmetric C-H stretching of CH_3
2940-2915	2931	2935	2931	Asymmetric C-H stretching of CH_2
1698-1690	1697	1697	1697	Antiparallel β -sheet
1695-1610	1621	1620	1621	<u>Amide I</u> C=O stretching and a small contribution from N-H bending (scissoring)

Table 4.4 (continued) Peak assignments of silk fibroin nanoparticles [18, 29-37].

Wavenumber (cm ⁻¹)	Current Work			Peak Assignments
	Methanol	Ethanol	<i>iso</i> - Propanol	
1575-1480	1514	1515	1514	<u>Amide II</u> N-H bending (wagging) plus C-N stretching
1480-1440	1444	1444	1444	C-H bending (scissoring) of CH ₂
1410-1350	1407	1408	1408	C-H bending (wagging) of CH ₃
1305-1200	1260,1229	1261,1230	1262,1230	<u>Amide III</u> N-H bending (twisting) plus C-N stretching and the contribution from O=C-N bending
1175-1165	1166	1166	1167	O-H bending of phenolic residue in Tyr
1100-1050	1066	1065	1066	C-N stretching of RCH ₂ - NH ₂ , R ₂ CH-NH ₂
1060-900	998, 975	997, 976	998, 976	C-C skeletal of Gly-Ala sequences

ศูนย์วิทยทรัพยากร
จุฬาลงกรณ์มหาวิทยาลัย

4.4 The secondary structure analysis of silk fibroin by ATR FT-IR microspectroscopy

4.4.1 Comparison of virgin silk fiber and degummed silk fiber (silk fibroin fiber)

Figure 4.9 shows the spectra of sericin gum, single virgin silk fiber and single degummed silk fiber. Each observed spectrum shows the different peak shape and peak positions. The IR peak assignments are summarized in Table 4.5.

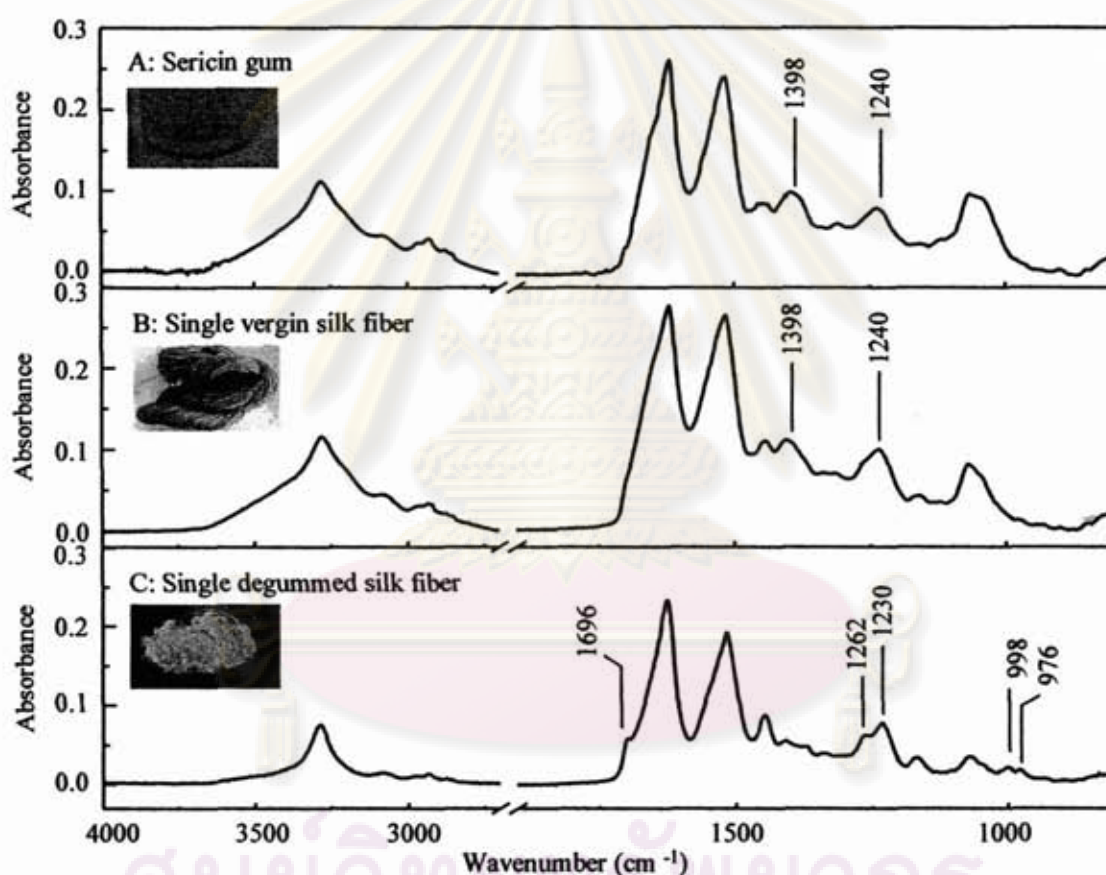


Figure 4.9 Comparison of ATR FT-IR spectra of silk: (A) sericin gum, (B) single virgin silk fiber, and (C) single degummed silk fiber. The spectra were acquired by the Ge slide-on IRE.

Sericin gum is mainly made of serine and threonine (polar amino acid), which can absorb the water molecules. Silk fibroin fiber is mainly composed of glycine and alanine (non-polar amino acid). The surface of silk fibroin fiber was coated with

sericin gum. This fiber was called *virgin silk fiber* and silk fibroin fiber was called *degummed silk fiber*. The spectra of single virgin silk fiber are similar to that of the spectra of sericin gum. As shown in Figure 4.9, the N-H stretching bands of sericin gum and single virgin silk fiber are broader than that of single degummed silk fiber. This broad band is due to the water molecules absorbed in molecular structure of sericin gum and single virgin silk fiber. As shown in Figure 4.9 (C), the weak band at 1696 cm^{-1} is assigned to the antiparallel β -sheet structure. This peak did not appear in the spectrum of single virgin silk fiber. It is noticed that the observed spectra of single virgin silk fiber and single degummed silk fiber in Amide I region are significantly different. The Amide I band of single degummed silk fiber is sharper than that of single virgin silk fiber because of the increasing of the crystalline structure. As shown in Figure 4.9 (B), the weak band at 1398 cm^{-1} is assigned to O-H bending vibration of serine amino acid. This peak did not appear in the spectrum of single degummed silk fiber because serine content in degummed silk fiber is only 12.1%. Single virgin silk fiber is the mainly composed of serine amino acid (approximately 31.97%), which has strongly polar side group (hydroxyl). The weak absorption band at 998 and 976 cm^{-1} are assigned to the Gly-Ala sequences. On the other hand, these peaks did not appear in single virgin silk fiber because glycine and alanine content of virgin silk fiber are approximately 12.7% and 5.51%, respectively. Single degummed silk fiber which is the mainly composed of non-polar amino acids such as glycine and alanine are approximately 44.6% and 29.4%, respectively. The single Amide III band of virgin silk fiber at 1240 cm^{-1} is assigned to unordered structure. Contrarily speaking, the Amide III band centered at 1230 cm^{-1} of degummed silk fiber showed a weak shoulder at 1262 cm^{-1} . These are assigned to the crystalline structure [15].

ศูนย์วิทยทรัพยากร
จุฬาลงกรณ์มหาวิทยาลัย

Table 4.5 Peak assignments of single silk fiber and degummed single silk fiber [18, 29-37].

Wavenumber (cm^{-1})	Current Work		Peak Assignments
	Silk fiber	Degummed silk fiber	
3385-3160	3271	3282	Symmetric N-H stretching
1698-1690 (w)	-	1696	Antiparallel β -sheet
1695-1610 (s)	1618	1624	<u>Amide I</u> C=O stretching and a small contribution from N-H bending (scissoring)
1575-1480 (s)	1514	1514	<u>Amide II</u> N-H bending (wagging) plus C-N stretching
1480-1440 (m)	-	1445	C-H bending (scissoring) of CH_2
1440-1260 (m, s)	1398	-	In plane of O-H bending
1410-1350 (m, s)	-	1407	C-H bending (wagging) of CH_3
1305-1200 (w, m)	1240	1262, 1230	<u>Amide III</u> N-H bending (twisting) plus C-N stretching and the contribution from O=C-N bending
1175-1165 (s)	1166	1166	O-H bending of phenolic residue in Tyr
1100-1050 (m)	-	1069	C-N stretching of $\text{RCH}_2\text{-NH}_2$, $\text{R}_2\text{CH-NH}_2$
1090-1000 (s)	1067	-	C-OH stretching
1060-900 (w, m)	-	998, 976	C-C skeletal of Gly-Ala sequences

The information of secondary structure of virgin silk fiber and degummed silk fiber were acquired by curve fitting analysis. The second-derivative spectra of virgin silk fiber and degummed silk fiber are shown in Figure 4.10 and the peak positions from the second-derivative spectra were used as parameter for curve fitting analysis in

Amide I region. The peak positions of the second-derivative spectra were choosing for curve fitting analysis.

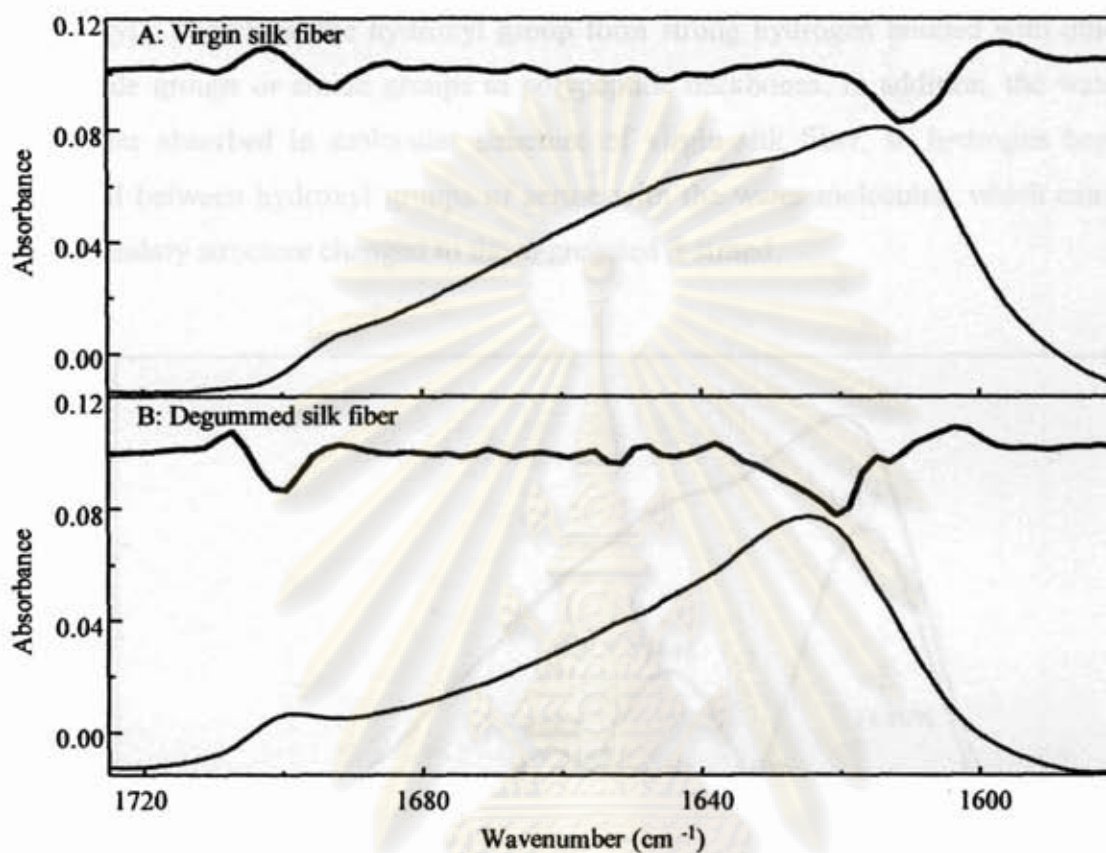


Figure 4.10 ATR FT-IR spectra of a single silk fiber in the Amide I region (bottom) with the corresponding second-derivative spectra (top): (A) Virgin silk fiber and (B) Degummed silk fiber.

Figures 4.11 and 4.12 show the curve fitting of single virgin silk fiber and single degummed silk fiber in Amide I region. The Amide I region in the spectra of virgin silk fiber and degummed silk fiber were fitted with Gaussian and Lorentzian functions to explain the secondary structure. The Amide I region are contributed from the C=O stretching vibration and N-H bending vibration mode in hydrogen-bonding pattern. The centers of the absorption bands are shown in Table 4.6. The proportion of each of the absorption bands was calculated as the percentage of a peak area. According to the fitted results, degummed silk fiber has more β -sheet structure than virgin silk fiber. In addition, virgin silk fiber has more random coil structure than degummed silk fiber. These results indicated that the secondary structure of degummed silk fiber had more crystalline structure than that of virgin silk fiber. The characteristic of the aggregated

β -strand was appeared after the curve fitting of virgin silk fiber. The aggregated β -strand has strong interchain interaction from polar side chains. The main components of virgin silk fiber are serine amino acid, which have strongly polar side group (hydroxyl). Therefore, the hydroxyl group form strong hydrogen bonded with other polar side groups or amide groups in polypeptide backbones. In addition, the water molecules absorbed in molecular structure of virgin silk fiber, so hydrogen bond occurred between hydroxyl groups of serine with the water molecules, which cause the secondary structure changed to the aggregated β -strand.

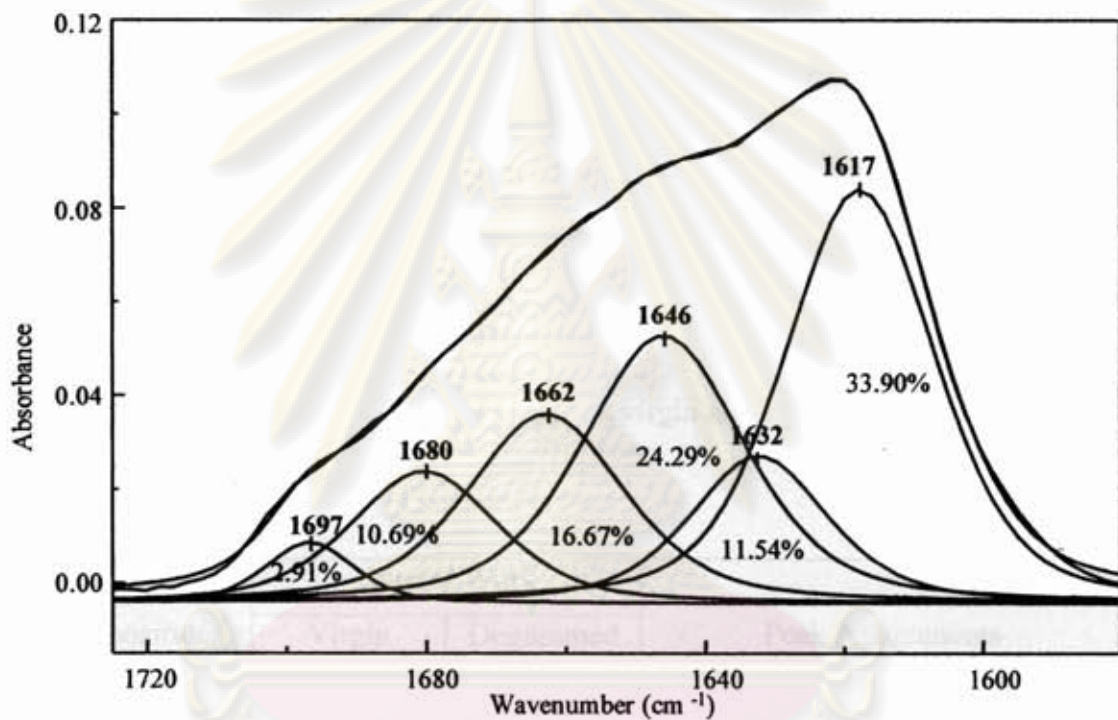


Figure 4.11 Curve fitting of spectrum of single virgin silk fiber in the Amide I region.

ศูนย์วิทยทรัพยากร
จุฬาลงกรณ์มหาวิทยาลัย

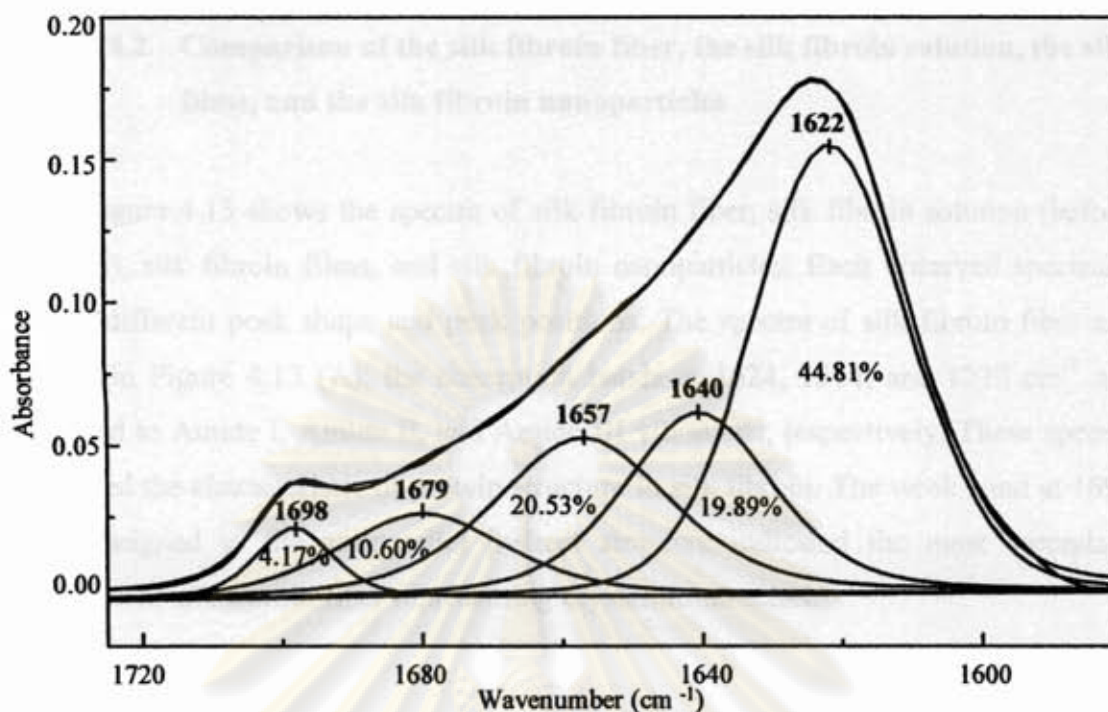


Figure 4.12 Curve fitting of spectrum of single degummed silk fiber in the Amide I region.

Table 4.6 The secondary structure of single virgin silk fiber and single degummed silk fiber [38-41].

Peak positions (cm^{-1})	Current Work		Peak Assignments
	Virgin silk fiber	Degummed silk fiber	
1703-1697	1697	1698	Intermolecular H-bonds of anti-parallel β -sheet (caused by the strong transition dipole coupling)
1696-1671	1680	1679	β -turn
1662-1656	1662	1657	α -helix
1655-1638	1646	1640	Random coil
1637-1628	1632	-	Intramolecular H-bonds of anti-parallel β -sheet
1627-1622	-	1622	Intermolecular H-bonds of anti-parallel β -sheet
1621-1616	1617	-	Aggregate β -strand

4.4.2 Comparison of the silk fibroin fiber, the silk fibroin solution, the silk films, and the silk fibroin nanoparticles

Figure 4.13 shows the spectra of silk fibroin fiber, silk fibroin solution (before dialysis), silk fibroin films, and silk fibroin nanoparticles. Each observed spectrum shows different peak shape and peak positions. The spectra of silk fibroin fiber are shown in Figure 4.13 (A), the absorption bands at 1624, 1514, and 1230 cm^{-1} are assigned to Amide I, Amide II, and Amide III vibrations, respectively. These spectra indicated the characteristic of protein structure in silk fibroin. The weak band at 1696 cm^{-1} assigned to the antiparallel β -sheet structure indicated the most secondary structure of silk fibroin fiber representing crystalline structure.

The spectrum of silk fibroin solution is shown in Figure 4.13 (B) which is similar to the spectra of the water. The N-H stretching band of silk fibroin solution is broader than those of other spectra because the large amount of the water in silk fibroin solution. Since the LiBr remains in the structure of silk fibroin solution, this salt may be the cause of water molecules absorbed in the structure. The weak band at 1549 cm^{-1} indicated presence of silk protein in the solution.

The spectrum of silk fibroin films are shown in Figure 4.13 (C). From the spectra, it was found that the N-H stretching band at 3285 cm^{-1} is broader than that of silk fibroin fiber and silk fibroin nanoparticles. This broad band is due to the large amount of the water molecules absorbed in molecular structure of silk fibroin films. The Amide I band at 1640 cm^{-1} and the single Amide III band at 1234 cm^{-1} are broaden, which are attributed to the random coil structure [3, 37]. The weak band in range of 1698-1690 cm^{-1} did not appear in the spectra of silk fibroin films. This indicates that most of the secondary structure of silk fibroin films is in the form of amorphous structure.

The spectrum of the silk fibroin nanoparticles are shown in Figure 4.13 (D). Silk fibroin nanoparticles were precipitated in the organic solvent, which organic solvent can diffuse into silk fibroin structure. The organic solvent attracted water from silk fibroin molecule and induced the rearrangement of polypeptide chains of silk fibroin. Therefore, the N-H stretching band of silk fibroin nanoparticles is sharper than those

of silk fibroin films. The Amide I band of the spectrum of silk fibroin films at 1640 cm^{-1} was red-shifted to 1621 cm^{-1} comparing with silk fibroin nanoparticles because of the increasing of crystalline structure in the structure of silk fibroin nanoparticles. The weak band at 1697 cm^{-1} and the Amide I band at 1621 cm^{-1} are associated with crystalline structure.

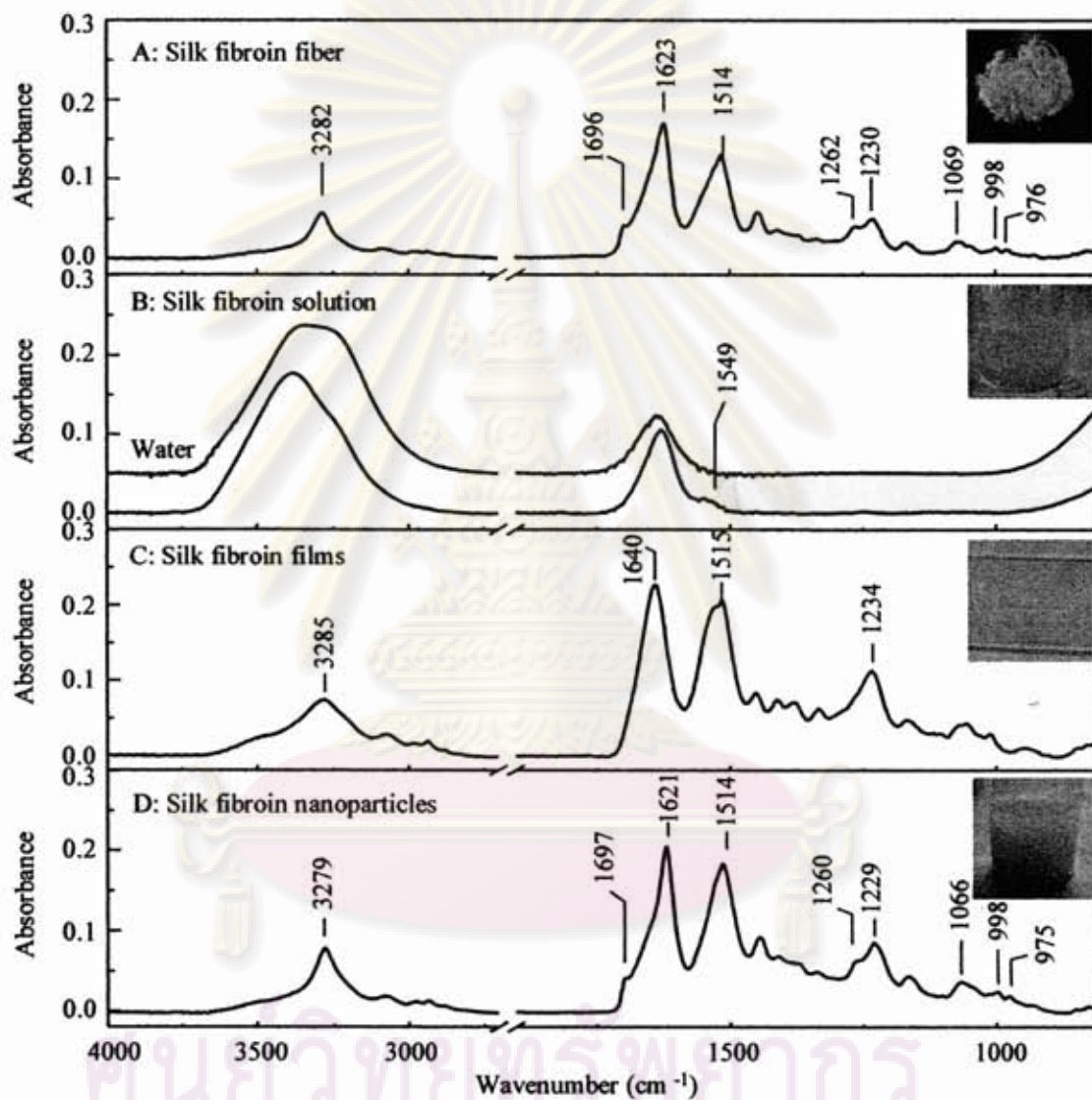


Figure 4.13 Comparison of ATR FT-IR spectra of silk: (A) silk fibroin fiber, (B) silk fibroin solution (before dialysis), (C) silk fibroin films, and (D) silk fibroin nanoparticles. The spectra were acquired by the Ge slide-on IRE. FT-IR spectra of water in Figure 4.13 (B) was added for comparison.

4.4.3 Comparison of the single silk fibroin fiber and the silk fibroin nanoparticles

The ATR FT-IR spectra of single silk fibroin fiber and silk fibroin nanoparticles precipitated in methanol, ethanol, and *iso*-propanol are shown in Figure 4.14, 4.15, 4.16, and 4.17, respectively. The spectra were collected at three different positions to ensure the reproducibility of the homemade slide-on Ge μ IRE. The observed spectra show that the tripple-collected spectra are identical as shown in the inset of Figure 4.14, 4.15, 4.16, and 4.17.

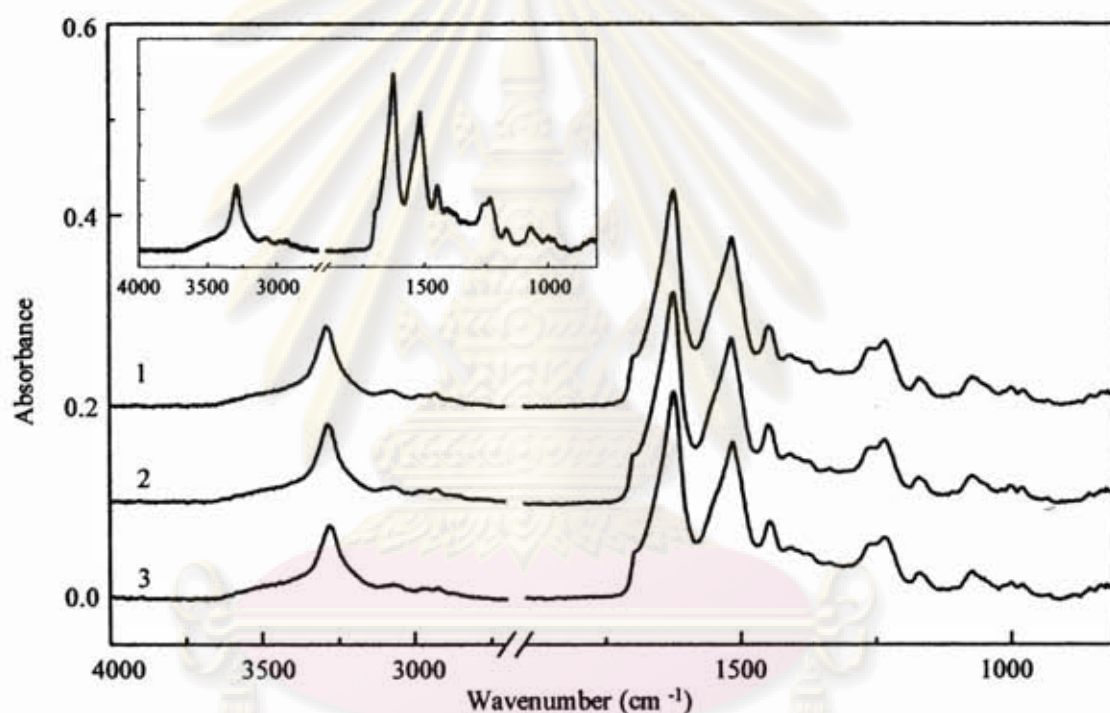


Figure 4.14 Normalized ATR FT-IR spectra of silk fibroin fiber.

ศูนย์วิทยทรัพยากร
จุฬาลงกรณ์มหาวิทยาลัย

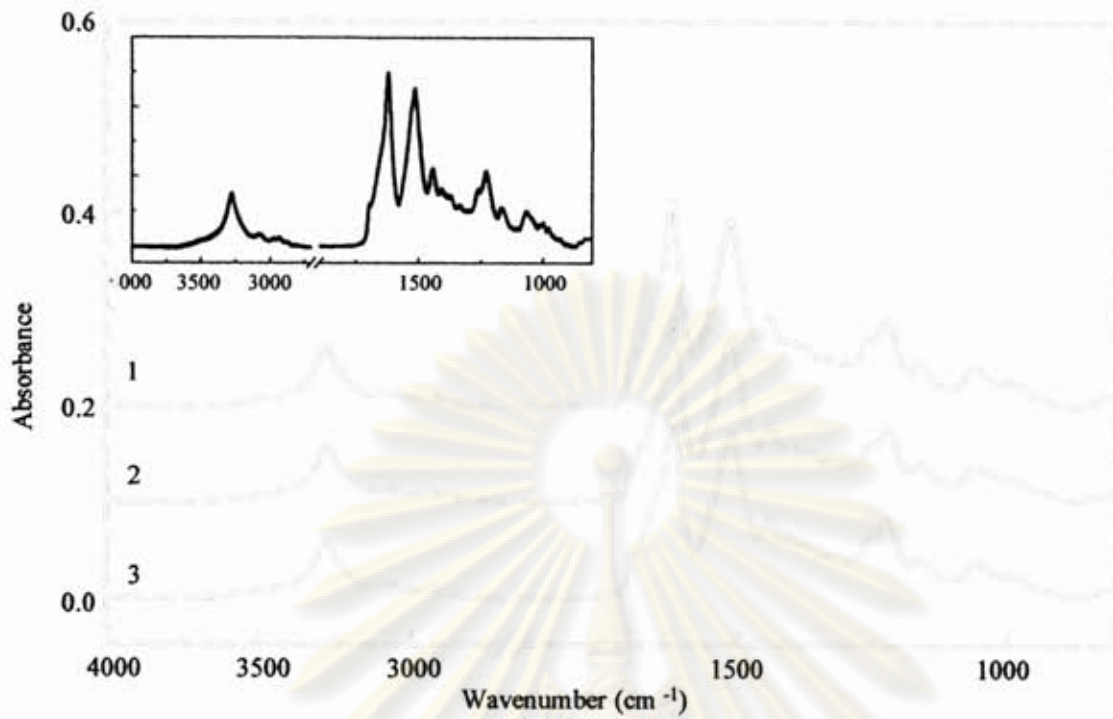


Figure 4.15 Normalized ATR FT-IR spectra of silk fibroin nanoparticles precipitated in methanol.

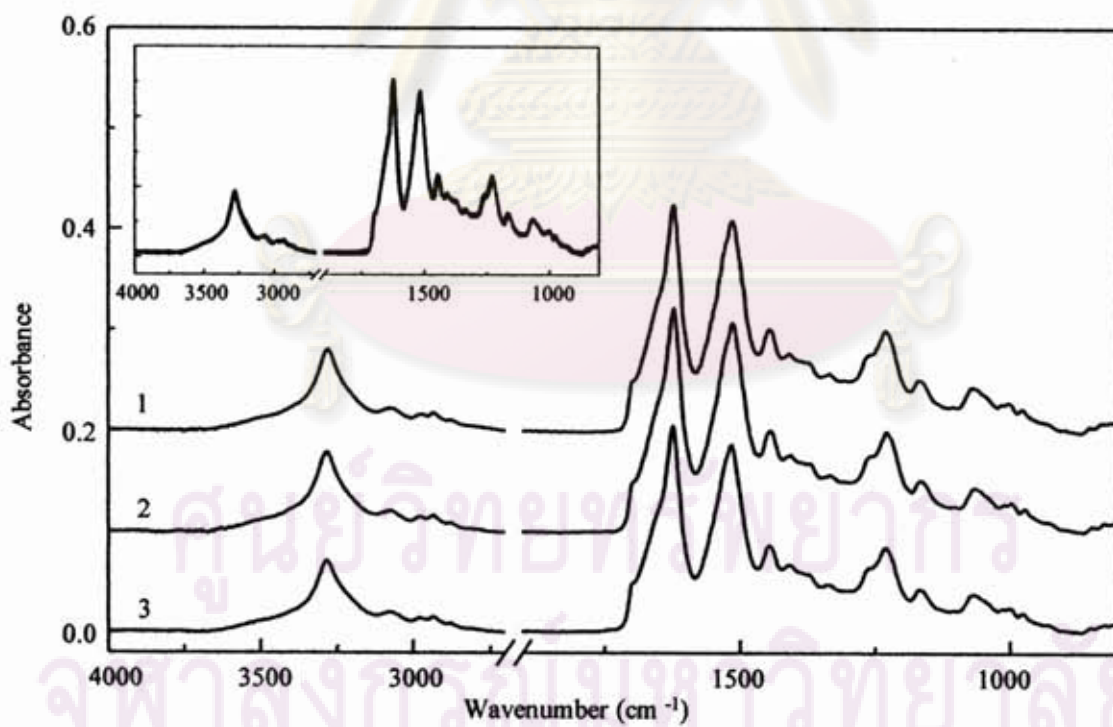


Figure 4.16 Normalized ATR FT-IR spectra of silk fibroin nanoparticles precipitated in ethanol.

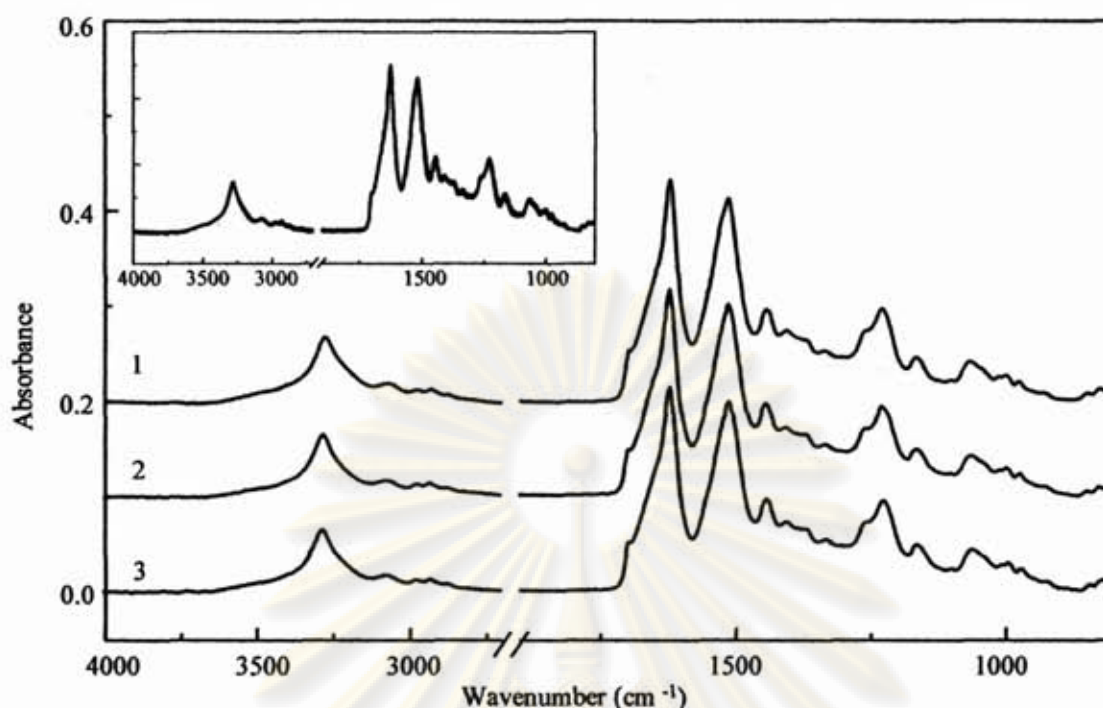


Figure 4.17 Normalized ATR FT-IR spectra of silk fibroin nanoparticles precipitated in *iso*-propanol.

The change of the secondary structure of silk fibroin nanoparticles was induced by precipitation of silk fibroin solution in organic solvents. The observed spectra of silk fibroin fiber and silk fibroin nanoparticles were compared in Figure 4.18. The spectra were normalized by N-H stretching band as shown in the inset A of Figure 4.18. The N-H stretching band of silk fibroin nanoparticles is broader than that of silk fibroin fiber. This broad band is due to the water molecules absorbed in molecular structure of silk fibroin nanoparticles. The organic solvent can diffuse into silk fibroin structure; the organic solvent attracts the water molecules from silk fibroin molecules and induces polypeptide chain rearrangement. The water molecules remain in molecular structure of silk fibroin nanoparticles. The inset B of Figure 4.18 shows the normalization of Amide I band. The different peak shape and peak positions in Amide I region (1623 cm⁻¹ in silk fibroin fiber and 1621, 1620, 1621 cm⁻¹ in silk fibroin nanoparticles precipitated in methanol, ethanol and *iso*-propanol, respectively.) reveal the change of the secondary structure in silk fibroin nanoparticles. For silk fibroin nanoparticles, all the absorption bands of Amide I bands are sharper than that of silk fibroin fiber. The Amide I bands of silk fibroin nanoparticles were red-shifted comparing with silk fibroin fiber because of the increasing of crystalline structure in the structure of silk fibroin nanoparticles. For silk fibroin nanoparticles, the peak

shifts of the Amide I band were similar to those of silk fibroin films treated by methanol [38]. The different peak shape in Amide I region implied the change of the secondary structure. So, the secondary structure of silk fibroin fiber and silk fibroin nanoparticles investigated further by mathematical curve fitting method in Amide I region.

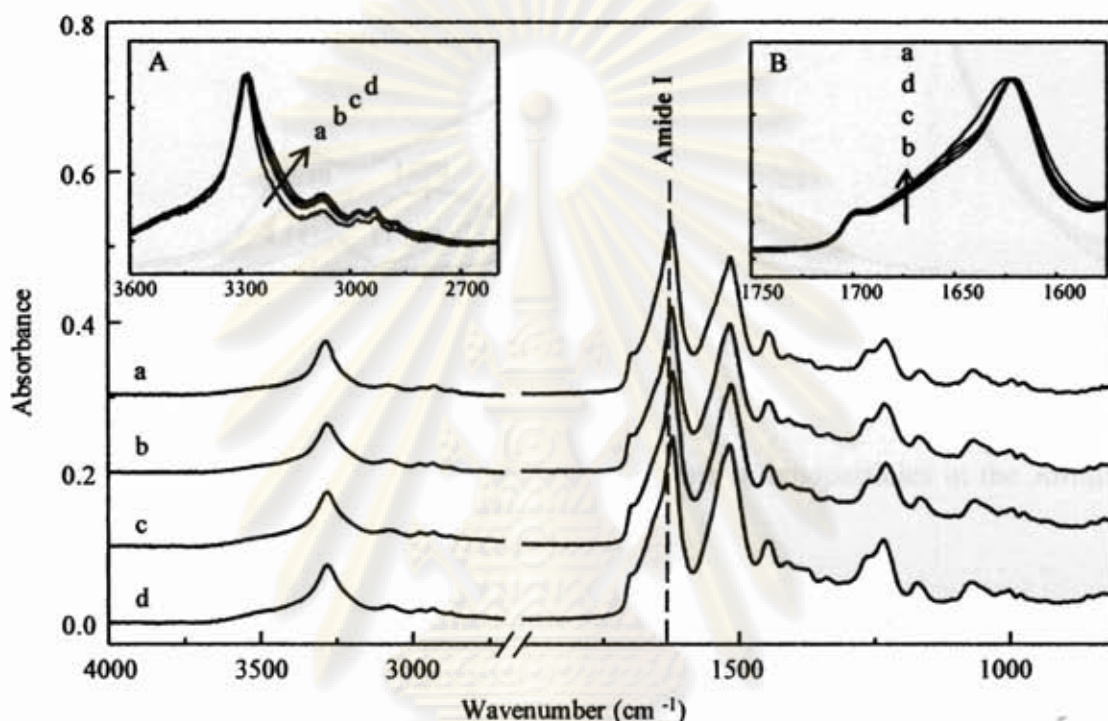


Figure 4.18 ATR FT-IR spectra of silk: (a) silk fibroin fiber, (b) silk fibroin nanoparticles precipitated in methanol, (c) silk fibroin nanoparticles precipitated in ethanol, and (d) silk fibroin nanoparticles precipitated in *iso*-propanol.

Figure 4.12 and 4.19, respectively, show the curve fitting of silk fibroin fiber and silk fibroin nanoparticles precipitated in methanol in Amide I region. The Amide I region in the spectra of silk fibroin fiber and silk fibroin nanoparticles were fitted with Gaussian and Lorentzian functions. The centers of the absorption band are shown in Table 4.7. According to the results, silk fibroin nanoparticles have smaller amount of α -helix and random coil structure than that of silk fibroin fiber while having greater amount of β -turn and β -sheet (1622 cm^{-1}) structure more than that of silk fibroin fiber. These indicated that the secondary structure of silk fibroin nanoparticles have more crystalline structure than that of silk fibroin fiber.

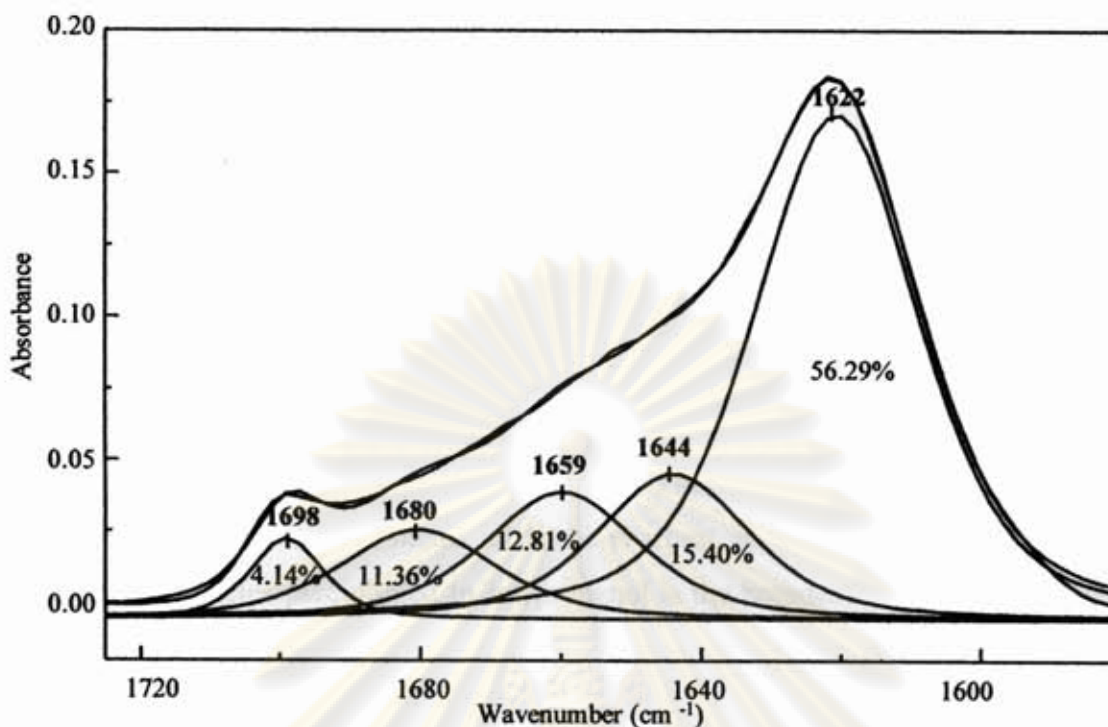


Figure 4.19 Curve fitting of spectrum of silk fibroin nanoparticles in the Amide I region.

Table 4.7 The secondary structure analysis of silk fibroin fiber and silk fibroin nanoparticles [38-41].

Peak positions (cm^{-1})	Current Work		Peak Assignments
	Silk fibroin fiber	Silk fibroin nanoparticles	
1703-1697	1698	1698	Intermolecular H-bonds of anti-parallel β -sheet (caused by the strong transition dipole coupling)
1696-1671	1679	1680	β -turn
1662-1656	1657	1659	α -helix
1655-1638	1640	1644	Random coil
1637-1622	1622	1622	Intermolecular H-bonds of anti-parallel β -sheet

4.4.4 Comparison of silk fibroin nanoparticles precipitated from different organic solvents

The organic solvents are well known as the crystallization reagent for silk fibroin molecules. The organic solvent types affected the secondary structure of silk fibroin. The observed spectra of silk fibroin nanoparticles precipitated in methanol, ethanol, and *iso*-propanol were compared in Figure 4.20. The observed spectrum shows different peak shape in Amide I region. The spectra were normalized by Amide I band as shown in the inset of Figure 4.20. The Amide I band of silk fibroin nanoparticles precipitated in methanol is the sharpest and the Amide I band of silk fibroin nanoparticles precipitated in *iso*-propanol is the broadest. The different peak shape in Amide I region implied the change of the secondary structure. Therefore, the investigation of the secondary structure of silk fibroin nanoparticles by mathematical curve fitting method in Amide I region was performed.

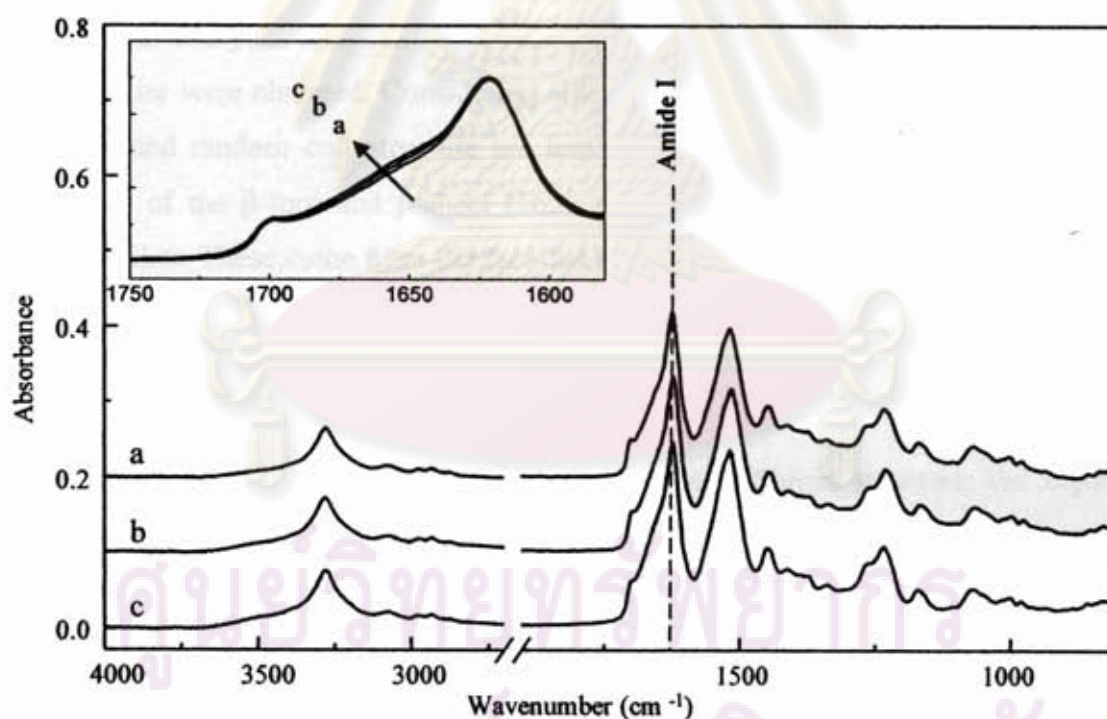


Figure 4.20 ATR FT-IR spectra of silk: (a) silk fibroin nanoparticles precipitated in methanol, (b) silk fibroin nanoparticles precipitated in ethanol, and (c) silk fibroin nanoparticles precipitated in *iso*-propanol.

Figure 4.21, 4.22, and 4.23, respectively, show the curve fitting of silk fibroin nanoparticles precipitated in methanol, silk fibroin nanoparticles precipitated in ethanol, and silk fibroin nanoparticles precipitated in *iso*-propanol in Amide I region. The Amide I region in the spectra of silk fibroin were fitted with Gaussian and Lorentzian functions. The centers of the absorption band are shown in Table 4.8. According to the results, silk fibroin nanoparticles precipitated in methanol were rich in the β -sheet (1622 cm^{-1}) structure. These indicated that the secondary structure of silk fibroin nanoparticles precipitated in methanol consisted of the crystalline structure more than that of silk fibroin nanoparticles precipitated in ethanol and *iso*-propanol. Silk fibroin nanoparticles precipitated in *iso*-propanol were rich in the random coil structure. These results indicated that the secondary structure of silk fibroin nanoparticles precipitated in *iso*-propanol consisted of the amorphous structure more than that of silk fibroin nanoparticles precipitated in methanol and ethanol. The observed curve fitting of silk fibroin fiber (Figure 4.12) and silk fibroin nanoparticles precipitated in three types of organic solvents (Figure 4.21, 4.22, and 4.23) were compared. The peak area contents of the α -helix, random coil, and β -sheet (1622 cm^{-1}) structure were changed. Considering silk fibroin nanoparticles, the contents of the α -helix and random coil structure are less than that of silk fibroin fiber while the contents of the β -turn and β -sheet (1622 cm^{-1}) structure is more than that of silk fibroin fiber. These come from the fact that the organic solvent induced the secondary changes of the molecular chains of silk fibroin from the random coil and α -helix to the β -turn and β -sheet structure.

Since the organic solvent can diffuse into silk fibroin structure, the organic solvent attracts the water molecules from silk fibroin molecules due to their polar character and induces the rearrangement of the molecular chains of silk fibroin from the random coil and α -helix to the β -sheet structure. After that the hydrophobic polypeptide chains were rearranged, the molecular conformations change to crystalline structure.

Silk fibroin nanoparticles precipitated in methanol have the highest β -sheet structure. Methanol is more polar than ethanol and *iso*-propanol. Therefore, methanol can attract water molecules from silk fibroin molecules. Then the hydrophobic polypeptide chains are induced to rearrange into closely packed form, and the

crystallization occurs [16, 42, 43]. The main components of crystalline region are composed of hydrophobic amino acids such as glycine and alanine. The sequence in this region is $-(\text{Gly-Ala-Gly-Ala-Gly-Ser})_n$. The amino acids in the sequence have non-polar side groups. Therefore, the molecular chain can be closely packed.

From Figure 4.13 (C and D), the Amide I band of silk fibroin films is broader than that of silk fibroin nanoparticles. The Amide I band of silk fibroin nanoparticles were red-shifted to 1621 cm^{-1} comparing to that of silk fibroin films (Figure 4.24). The different peak shape and peak positions in Amide I region implied the change of the secondary structure. In order to understand these difference; the investigation of the secondary structure of silk fibroin by mathematical curve fitting method in Amide I region was performed.

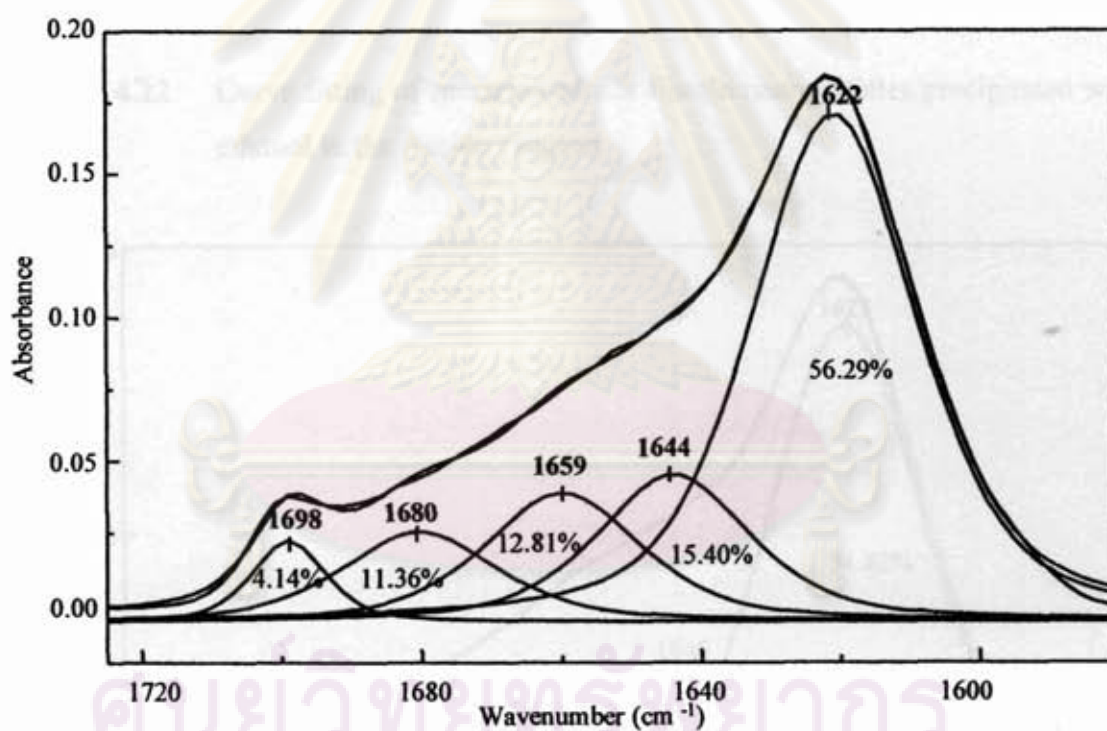


Figure 4.21 Curve fitting of spectrum of silk fibroin nanoparticles precipitated with methanol in the Amide I region.

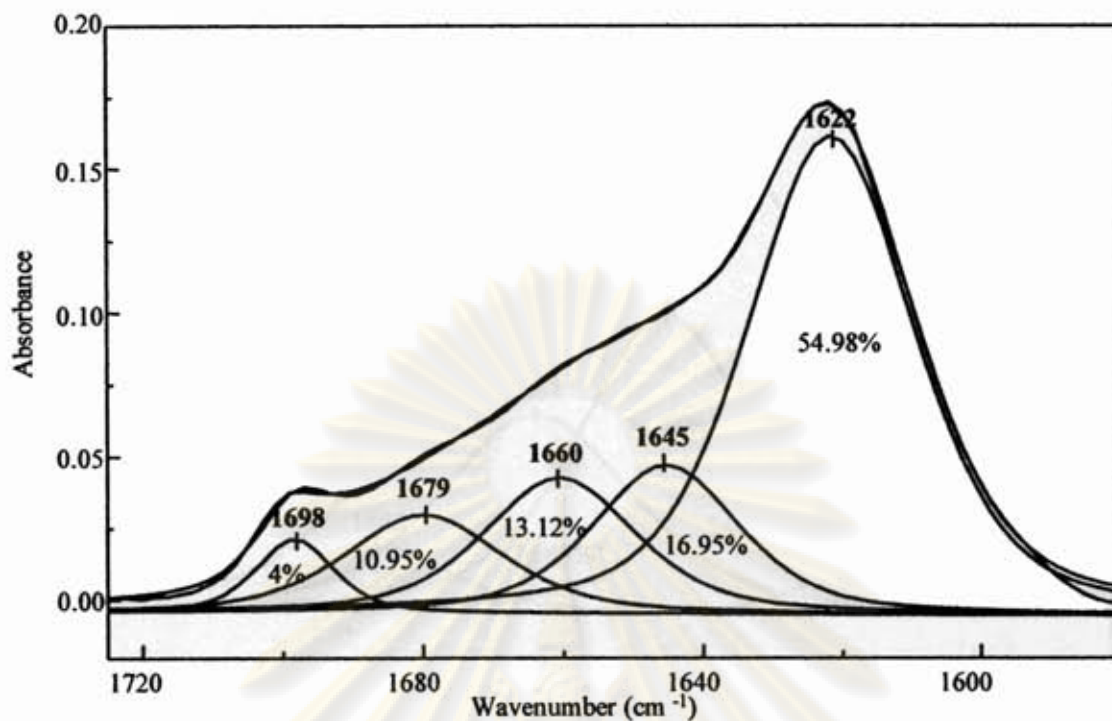


Figure 4.22 Curve fitting of spectrum of silk fibroin nanoparticles precipitated with ethanol in the Amide I region.

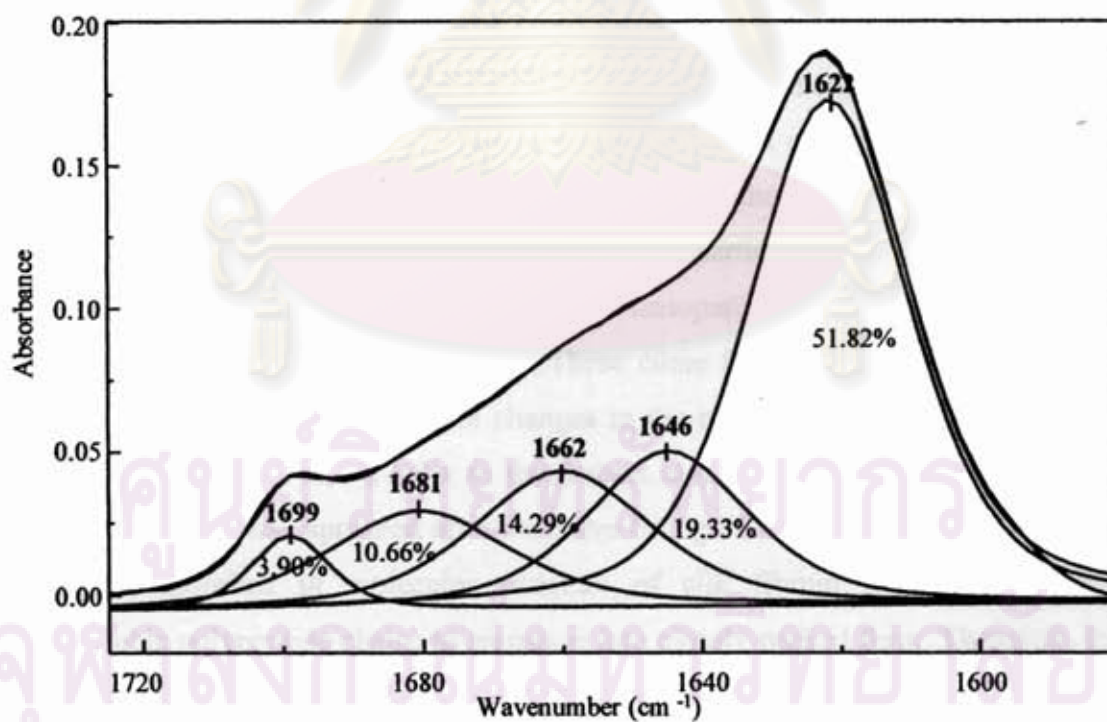


Figure 4.23 Curve fitting of spectrum of silk fibroin nanoparticles precipitated with *iso*-propanol in the Amide I region.

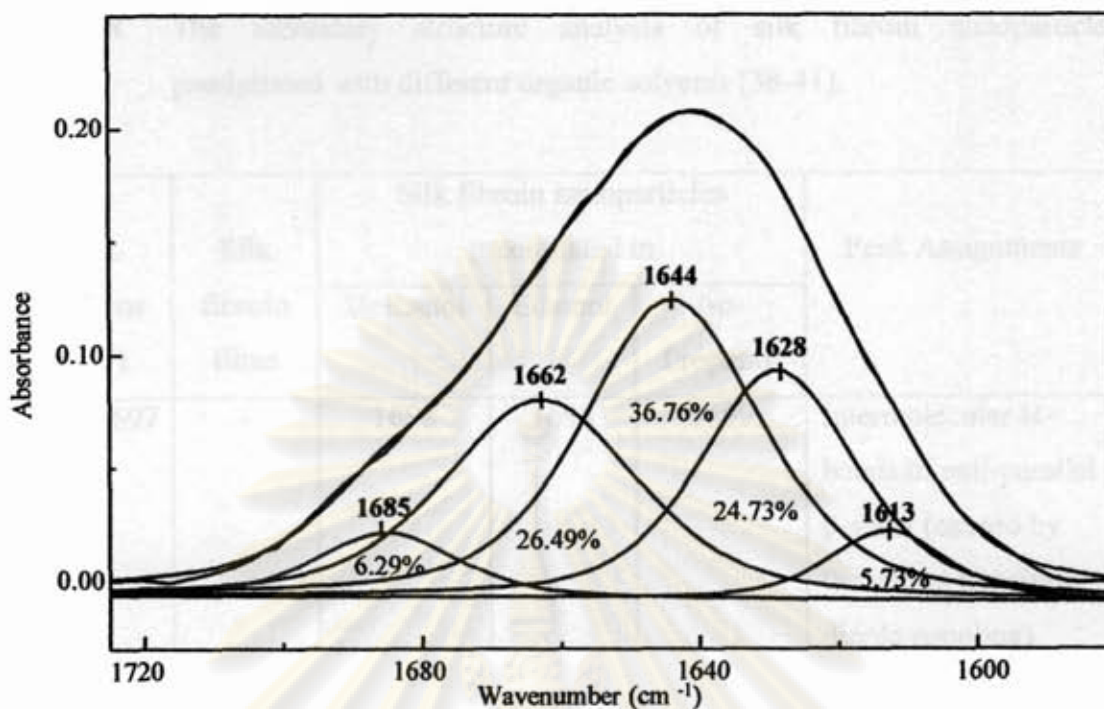


Figure 4.24 Curve fitting of spectrum of silk fibroin films in the Amide I region.

The observed curve fitting of silk fibroin nanoparticles precipitated in three types of organic solvents and silk fibroin films were compared. The area contents of the β -turn, α -helix, random coil, and β -sheet structure were changed. Considering silk fibroin films, the contents of the α -helix and random coil structure are greater than that of silk fibroin nanoparticles while the contents of the β -turn and β -sheet (1628 cm^{-1}) structure is lesser than that of silk fibroin nanoparticles. These results indicated that the secondary structure of silk fibroin nanoparticles have more crystalline structure than that of silk fibroin films. These come from the fact that the organic solvent induced secondary structure changes in the molecular chains of silk fibroin from the random coil and α -helix to the β -sheet structure. The characteristic of the aggregated strand was appeared after the curve fitting of silk fibroin films. The water molecules absorbed in molecular structure of silk fibroin films prevents the hydrophobic polypeptide chains to rearrange into closely packed form. Therefore, the secondary structure changed to the aggregated strand.

Table 4.8 The secondary structure analysis of silk fibroin nanoparticles precipitated with different organic solvents [38-41].

Peak positions (cm ⁻¹)	Silk fibroin films	Silk fibroin nanoparticles precipitated in			Peak Assignments
		Methanol	Ethanol	<i>iso</i> -Propanol	
1703-1697	-	1698	1698	1699	Intermolecular H-bonds of anti-parallel β -sheet (caused by the strong transition dipole coupling)
1696-1671	1685	1680	1679	1681	β -turn
1662-1656	1662	1659	1660	1662	α -helix
1655-1638	1644	1643	1645	1646	Random coil
1637-1622	1628	1622	1622	1622	Intermolecular H-bonds of anti-parallel β -sheet
1615-1605	1613	-	-	-	Aggregated strand

4.5 The deposition of silver nanoparticles on silk fibroin nanoparticles

Silver nanoparticles were deposited on silk fibroin nanoparticles. The deposition of silver nanoparticles was analyzed by UV-Visible spectrometer and TEM. The absorption spectra of silver nanoparticles before and after depositing on the silk fibroin nanoparticles monitored by UV-Visible spectrometer are shown in Figure 4.26 and their corresponding photographs shown in Figure 4.25.

จุฬาลงกรณ์มหาวิทยาลัย



Figure 4.25 Photograph of silver nanoparticles at different concentrations deposited on silk fibroin nanoparticles: (a) 50 ppm, (b) 100 ppm, and (c) 200 ppm.

Silver nanoparticles colloidal solutions have absorption maxima (λ_{\max}) at 400 nm. The silver nanoparticles were spherical shape and the mean diameter of particles was about 10 nm as shown in Figure 4.26.

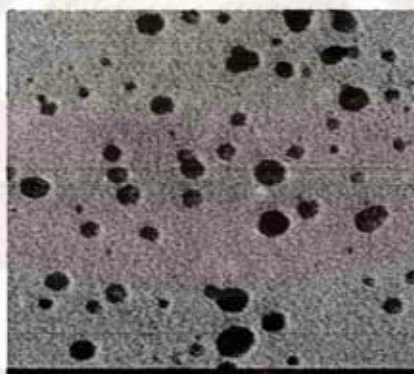


Figure 4.26 TEM images of silver nanoparticles colloidal solution.

The absorbance was not significantly changed in the position of the absorption maxima, which observed from normalization absorption spectra as shown in the inset of Figure 4.27 (A, B, and C). The absorbance of silver nanoparticles deposited on the silk fibroin nanoparticles increased with increasing the concentration of silver nanoparticles. From these results, silver nanoparticles could deposit on silk fibroin nanoparticles, which observed from the decreasing absorption spectra of silver

nanoparticles colloidal solution after silver nanoparticles were added into silk fibroin nanoparticles.

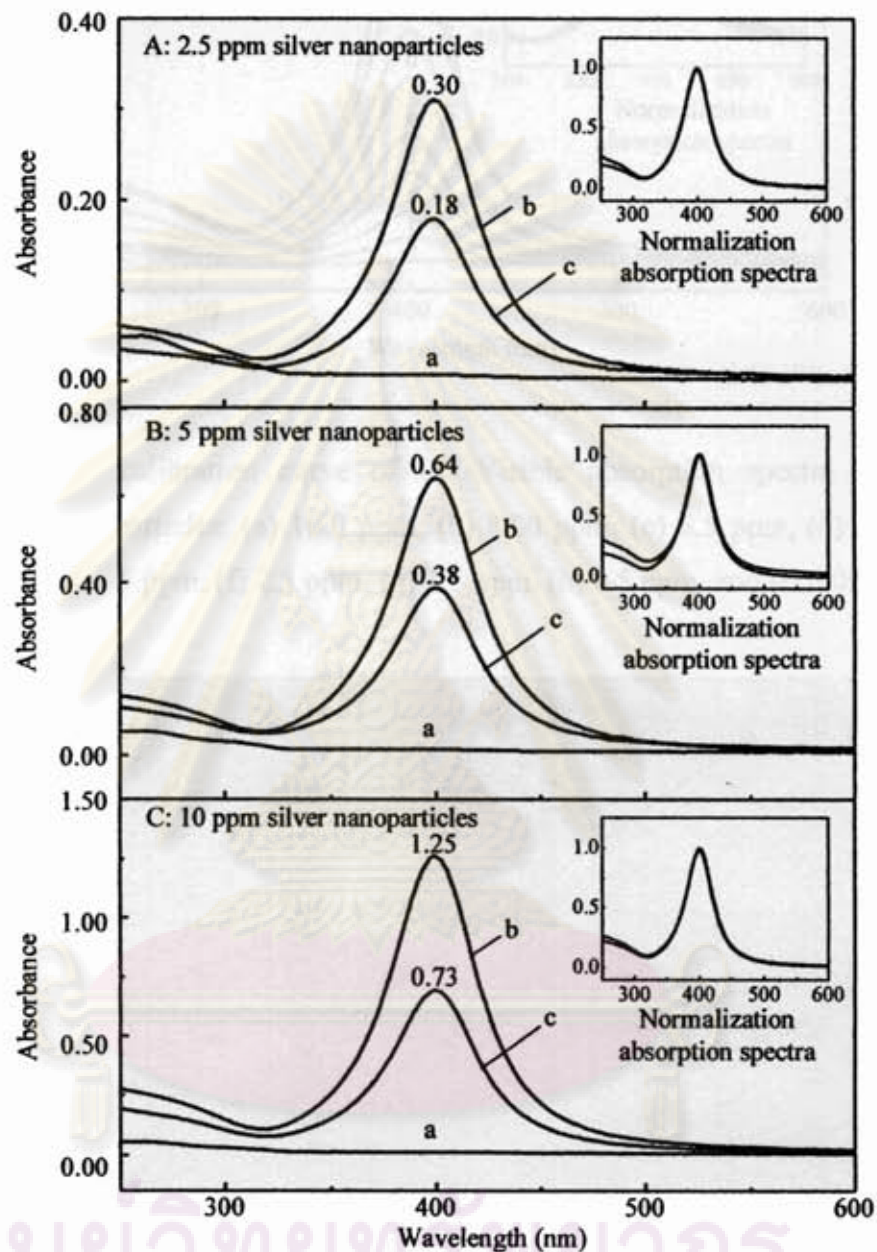


Figure 4.27 The UV-Visible absorption spectra of silver nanoparticles: (a) silk fibroin nanoparticles, (b) before silver nanoparticles were added, and (c) after silver nanoparticles were added.

The weights of silver nanoparticles deposited on silk fibroin nanoparticles are calculated from the UV-Visible absorption spectra. From Figure 4.28, the plotting of intensity at absorption maxima against silver nanoparticles concentrations are shown in Figure 4.29.

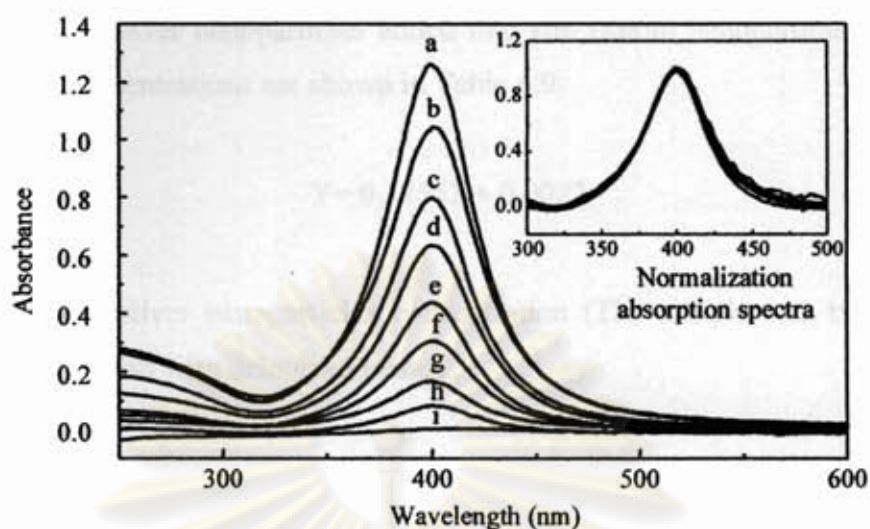


Figure 4.28 The calibration curve of UV-Visible absorption spectra of silver nanoparticles: (a) 10.0 ppm, (b) 8.00 ppm, (c) 6.5 ppm, (d) 5.0 ppm, (e) 3.5 ppm, (f) 2.5 ppm, (g) 1.5 ppm, (h) 0.5 ppm, and (i) 0.05 ppm.

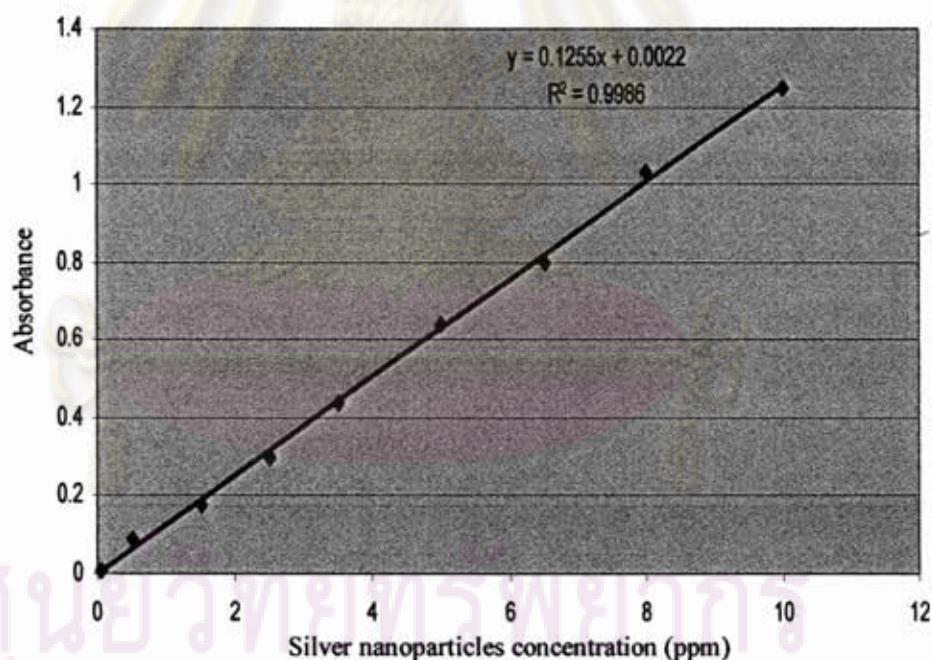


Figure 4.29 Plot of intensity at absorption maxima against silver nanoparticles concentrations (ppm).

The equation 4.2 was calculated from the plot of intensity at absorption maxima against silver nanoparticles concentrations, which was used to calculate the

concentration of silver nanoparticles added into silk fibroin nanoparticle. The silver nanoparticles concentrations are shown in Table 4.9.

$$Y = 0.1255X + 0.0022 \quad (4.2)$$

Table 4.9 The silver nanoparticles concentration (The sample was twenty times dilution with deionized water).

Silver nanoparticles colloidal solution (ppm)	Absorbance of silver nanoparticles (Y)			Silver nanoparticles concentration (X)		
	Before adding	Remain in supernatant	Deposited on silk	Before adding	Remain in solution	Deposited on silk
2.50	0.308	0.184	0.124	2.436	1.448	0.970
5.00	0.643	0.381	0.262	5.105	3.018	2.070
10.00	1.259	0.738	0.521	10.010	5.862	4.133

10 mL of 50, 100, and 200 ppm silver nanoparticles colloidal solution were added into silk fibroin nanoparticles suspension (0.055 ± 0.010 g). The weight of silver nanoparticles deposited on silk fibroin nanoparticles can be calculated as follows:

$$\text{weight}(\mu\text{g}) = \text{silver concentration (ppm)} \times \text{volume of silver solution (mL)} \quad (4.3)$$

Volume of silver nanoparticles solution = 10.00 mL

For example:

At 2.5 ppm silver nanoparticles colloidal solution, they were deposited on silk fibroin nanoparticles 0.970 ppm. The weight of silver nanoparticles calculated as follows:

$$\begin{aligned} \text{weight}(\mu\text{g}) &= 0.970 \times 10.00 \\ &= 9.70 \end{aligned}$$

Weight of silver nanoparticles deposited on silk fibroin nanoparticles were calculated from equation 4.2 was shown in Table 4.10 and Table 4.11. From this

result, the weight of silver nanoparticles deposited on silk fibroin nanoparticles increased with increasing the concentration of silver nanoparticles. These results indicated that the system occurred at equilibrium of silver nanoparticles between solid phase and liquid phase, which confirmed by soaking silver-deposited silk fibroin nanoparticles in deionized water.

Table 4.10 Weight of silver nanoparticles deposited on silk fibroin nanoparticles (The sample was twenty times dilution with deionized water).

Silver nanoparticles colloidal solution (ppm)	Weight (μg) of silver nanoparticles deposited on silk fibroin nanoparticles	Weight (μg) of silver nanoparticles deposited on silk fibroin nanoparticles
	0.055 g	1.00 g
2.50	9.70	176.36
5.00	20.70	376.36
10.00	41.33	751.45

Table 4.11 Weight of silver nanoparticles deposited on silk fibroin nanoparticles.

Silver nanoparticles colloidal solution (ppm)	Deposition of silver nanoparticles (μg) / silk nanoparticles 1.00 g
50	3527.27
100	7527.27
200	15029.09

The equilibrium of silver nanoparticles was tested by adding 20 mL of the deionized water into 0.055 g of silver-deposited silk fibroin nanoparticles of 50 ppm, 100 ppm, and 200 ppm, respectively. After that silver-deposited silk fibroin nanoparticles were released. The UV-visible spectra of the deionized water were measured. The concentrations of silver nanoparticles were then calculated from the calibration curve. The absorption spectra of released silver nanoparticles from silk

fibroin nanoparticles are shown in Figure 4.30 and the amount of silver nanoparticles released from silk fibroin nanoparticles are shown in Table 4.12.

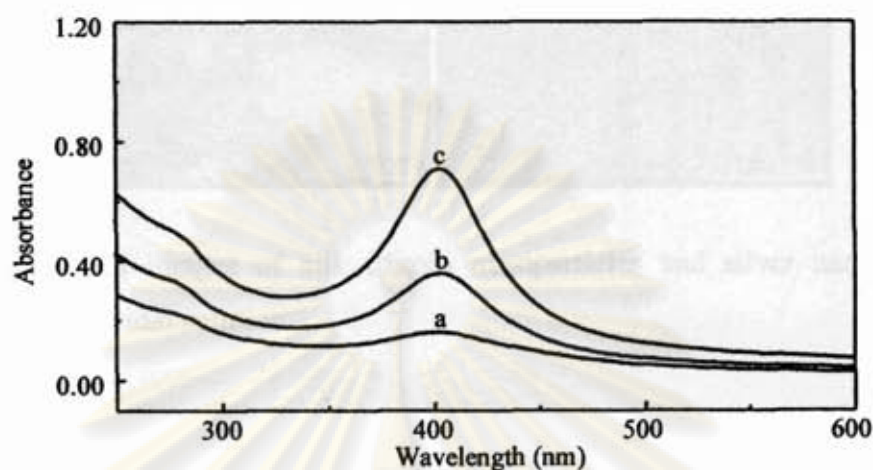


Figure 4.30 The UV-Visible absorption spectra released silver nanoparticles from silk fibroin nanoparticles: (a) 50 ppm, (b) 100 ppm, and (c) 200 ppm.

Table 4.12 Weight of silver nanoparticles released from silk fibroin nanoparticles.

Silver nanoparticles colloidal solution (ppm)	Weight (μg) of silver nanoparticles release / silk fibroin nanoparticles 1.00 g
50	457.20
100	1036.69
200	2021.85

4.5.1 TEM images of silver nanoparticles and silver-deposited silk fibroin nanoparticles.

TEM images of silk fibroin nanoparticles, silver nanoparticles, and silver-deposited silk fibroin nanoparticles as shown in Figure 4.31 and 4.32, respectively.

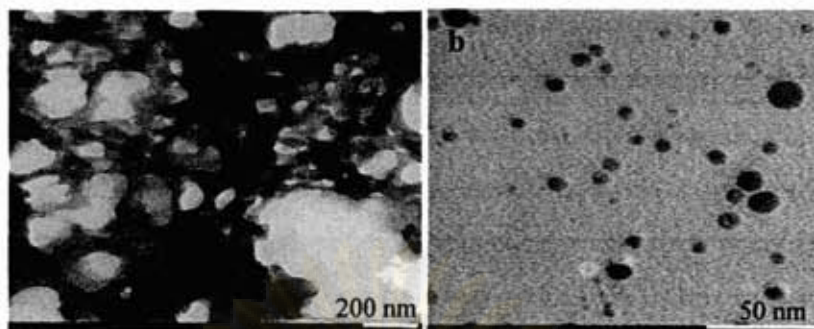


Figure 4.31 TEM images of silk fibroin nanoparticles and silver nanoparticles colloidal solution.

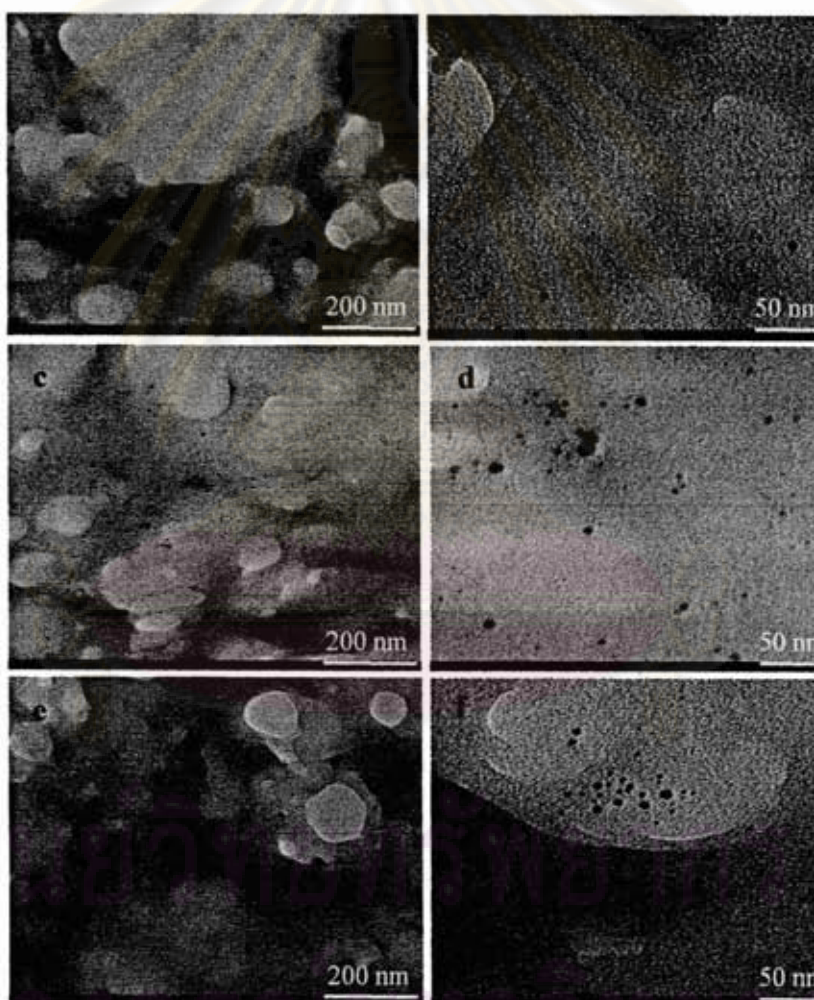


Figure 4.32 TEM images of silk fibroin nanoparticles deposited with silver nanoparticles: (a) and (b) deposited at 50 ppm; (c) and (d) deposited at 100 ppm; and (e) and (f) deposited at 200 ppm.

From these results, it is concluded that silver nanoparticles are well dispersed and well deposited on silk fibroin nanoparticles. The deposition of 200 ppm silver nanoparticles on the silk fibroin nanoparticles is more than those of 100 ppm and 50 ppm silver nanoparticles, respectively. The deposition of silver nanoparticles on silk fibroin nanoparticles decreased with decreasing the concentration of silver nanoparticles, which were also in a good agreement with the results UV-Visible absorption spectra.

4.5.2 Comparison of silk fibroin nanoparticles and silver-deposited silk fibroin nanoparticles.

Figure 4.33 shows ATR FT-IR spectra of silver-deposited silk fibroin nanoparticles. The spectrum of silk fibroin nanoparticles are shown in Figure 4.33 (A). The absorption bands of Amide I, Amide II, and Amide III vibrations indicated the characteristic of silk fibroin protein structure. The spectra of silver-deposited silk fibroin nanoparticles are shown in Figure 4.33 (B, C, and D). Each observed spectrum shows the absorption bands at 1749 cm^{-1} . It is assigned to the C=O group, which is only weakly hydrogen bond [44]. These absorption bands did not appear in the spectrum of silk fibroin nanoparticles. It is possible that during silver nanoparticles are filled into silk fibroin nanoparticles, silver nanoparticles deposit on silk and insert between the β -sheet structures of silk fibroin structure. So, hydrogen bond is weak.

ศูนย์วิทยทรัพยากร
จุฬาลงกรณ์มหาวิทยาลัย

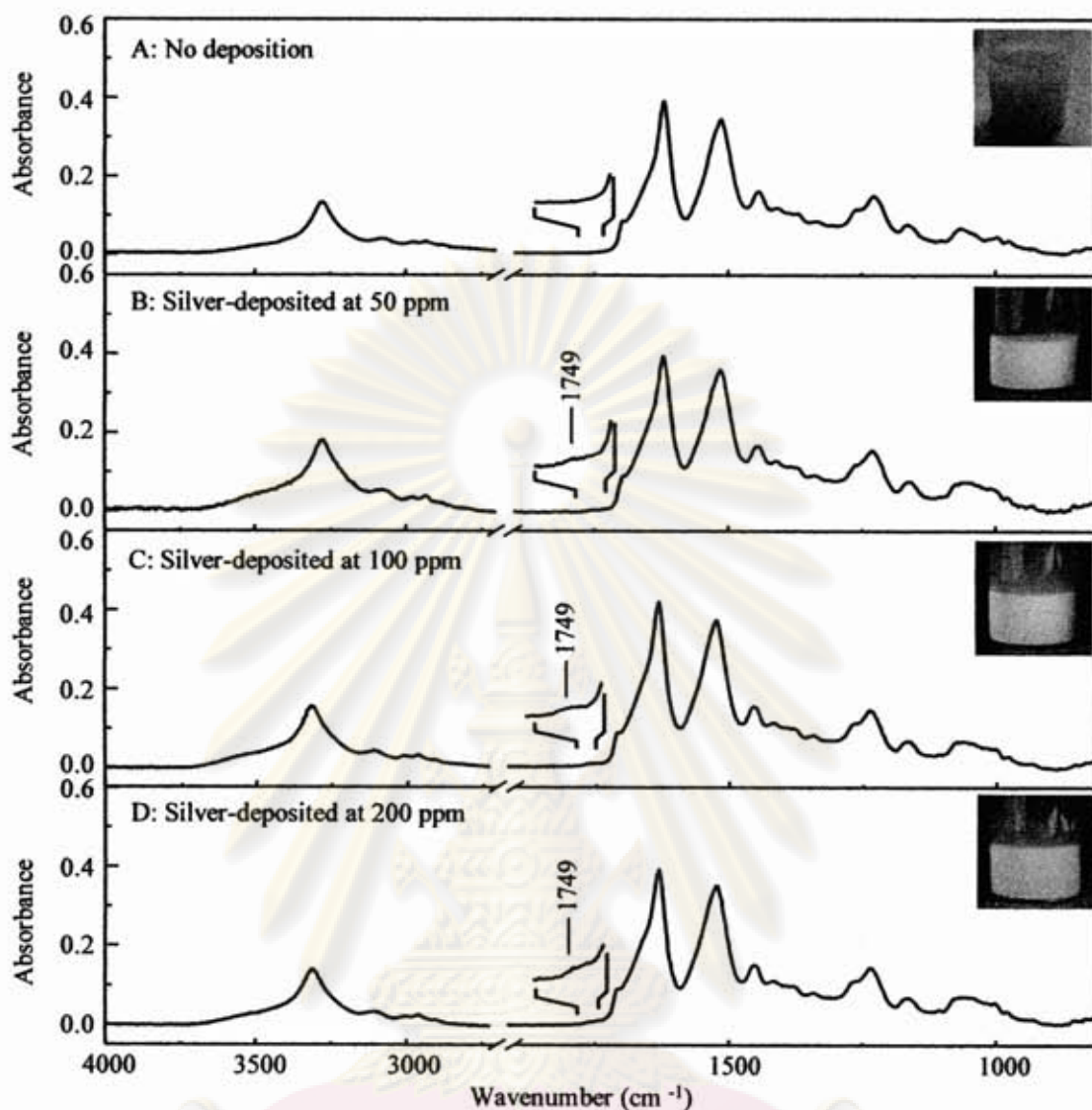


Figure 4.33 ATR FT-IR spectra of silk fibroin nanoparticles: (A) no silver-deposition, (B) silver-deposited at 50 ppm (C) silver-deposited at 100 ppm, and (D) silver-deposited at 200 ppm, respectively.

Figure 4.21, 4.34, 4.35, and 4.36 show the curve fitting of silk fibroin nanoparticles and silver-deposited silk fibroin nanoparticles in Amide I region. The information of secondary structure of silk fibroin nanoparticles were resolved by curve fitting analysis. The Amide I region between $1740\text{--}1580\text{ cm}^{-1}$ was fitted with Gaussian and Lorentzian functions. The centers of the absorption band are shown in Table 4.13.

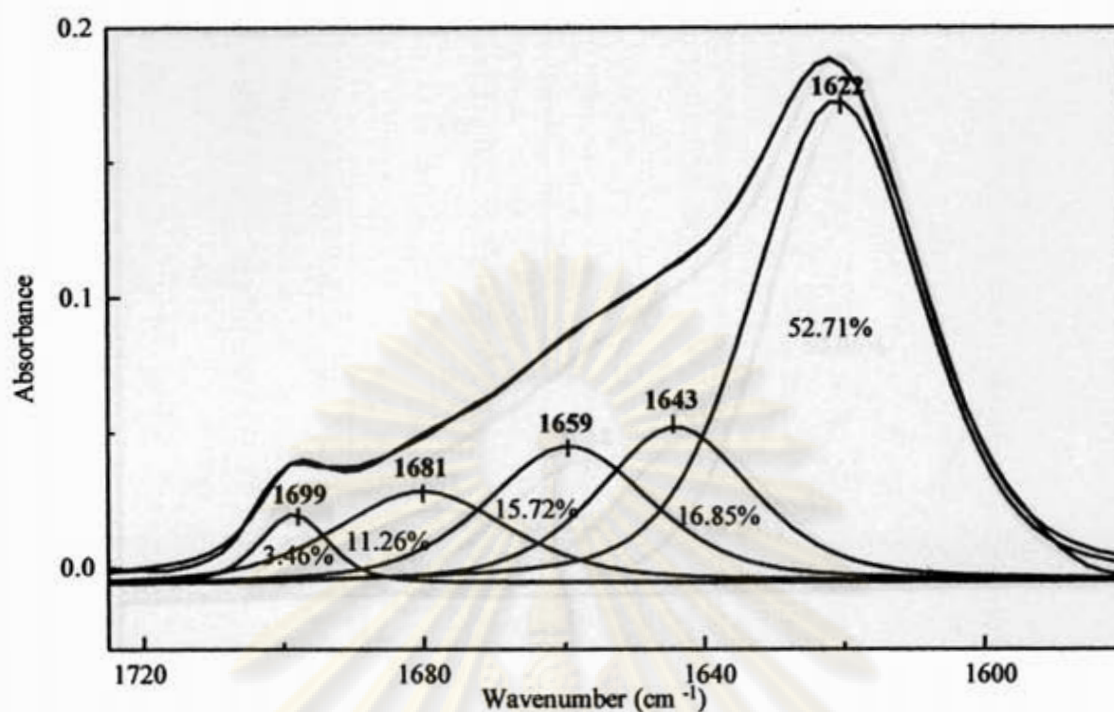


Figure 4.34 Curve fitting of spectrum of silver-deposited at 50 ppm in the Amide I region.

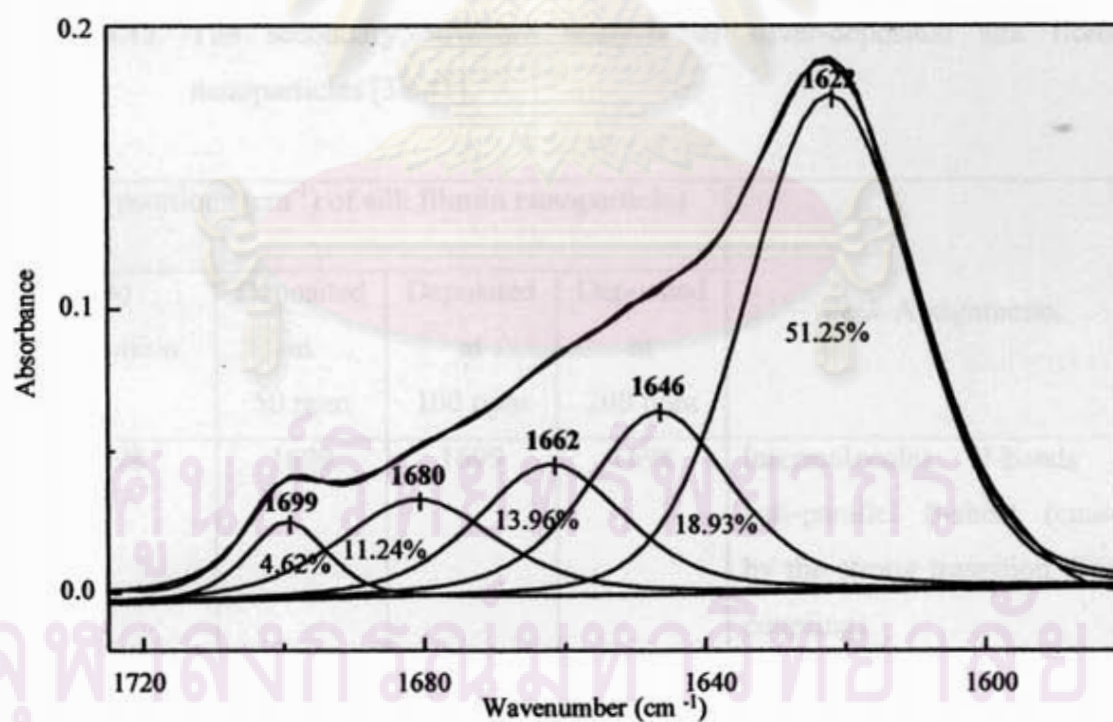


Figure 4.35 Curve fitting of spectrum of silver-deposited at 100 ppm in the Amide I region.

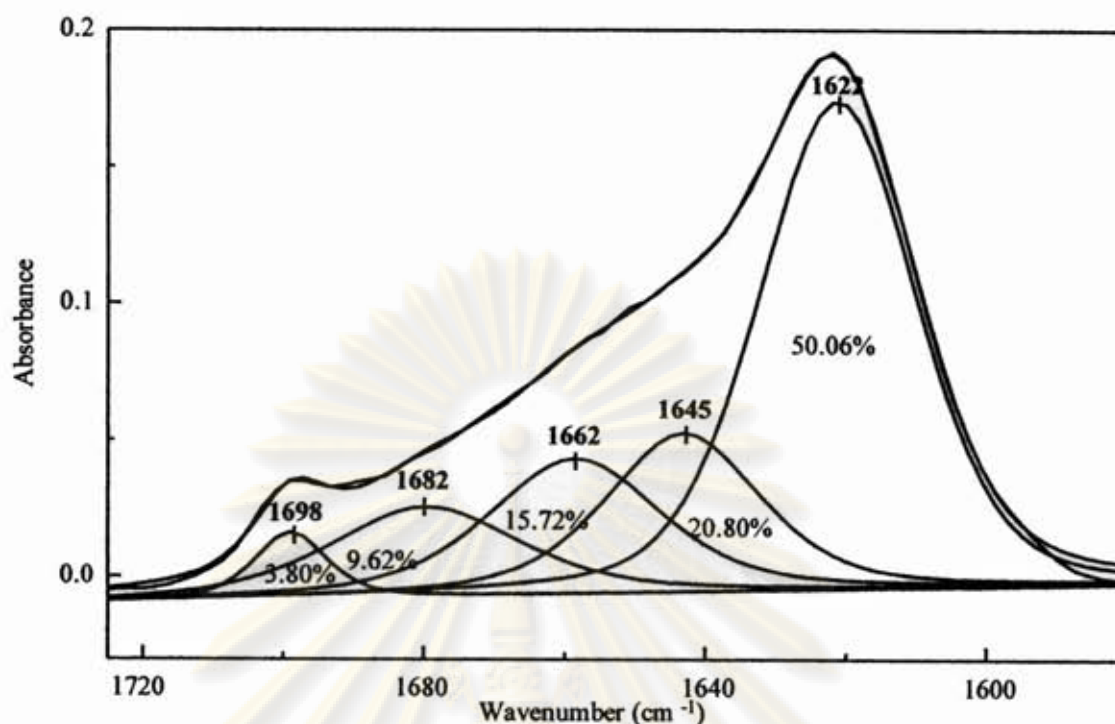


Figure 4.36 Curve fitting of spectrum of silver-deposited at 200 ppm in the Amide I region.

Table 4.13 The secondary structure analysis of silver-deposited silk fibroin nanoparticles [38-41].

Peak positions (cm^{-1}) of silk fibroin nanoparticles				Peak Assignments
No deposition	Deposited at 50 ppm	Deposited at 100 ppm	Deposited at 200 ppm	
1698	1699	1699	1698	Intermolecular H-bonds of anti-parallel β -sheet (caused by the strong transition dipole coupling)
1680	1681	1680	1682	β -turn
1659	1659	1662	1662	α -helix
1644	1643	1646	1645	Random coil
1622	1622	1622	1622	Intermolecular H-bonds of anti-parallel β -sheet

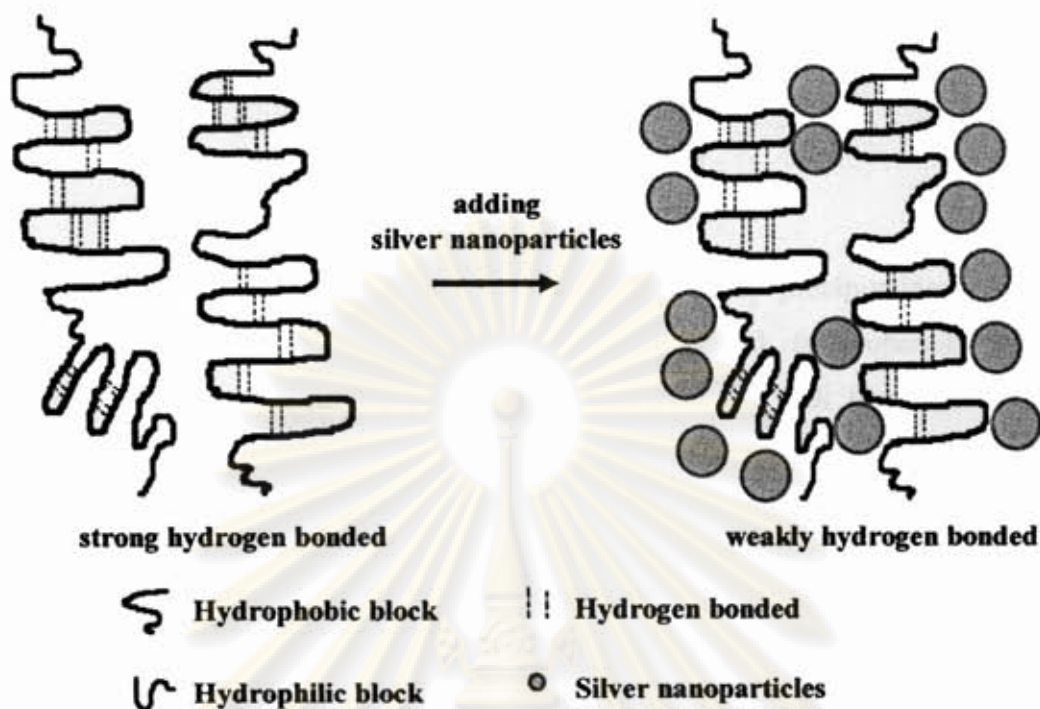


Figure 4.37 The proposed mechanism of silver nanoparticles inserted into the silk fibroin structures.

The observed curve fitting of silk fibroin nanoparticles and silver-deposited silk fibroin nanoparticles (50, 100, and 200 ppm) are compared. The area contents of the α -helix, random coil, and β -sheet (1622 cm^{-1}) structure were changed. Consider silver-deposited silk fibroin nanoparticles, the contents of the α -helix and random coil structures are more than that of silk fibroin nanoparticles while the contents of the β -turn and β -sheet (1622 cm^{-1}) structure are less than that of silk fibroin nanoparticles. These results indicated that the content of crystalline structure of silk fibroin was reduced and amorphous structure of silk fibroin was increased after silver nanoparticles were added. These may come from the possibility that silver nanoparticles can be inserted into the silk fibroin structures. The proposed mechanism of silver nanoparticles inserted into the silk fibroin structures is shown in Figure 4.37. Therefore, deposited silver nanoparticles prevent the hydrophobic polypeptide chains to rearrange into closely packed form.

CHAPTER V

CONCLUSIONS

Silk fibroin nanoparticles were simply prepared by precipitating silk fibroin solution in organic solvents (methanol, ethanol, and *iso*-propanol) at room temperature. The optimal final concentration of NaCl in silk fibroin solution for precipitating solution is 0.05 M. The optimum volume ratio of the silk fibroin solution per organic solvents was 16.6% v/v. From SEM images, silk fibroin nanoparticles have spherical shape and particles sizes of silk fibroin nanoparticles precipitated in methanol, ethanol, and *iso*-propanol on the average of 98.43 ± 2.9 , 92.73 ± 3.8 , and 98.60 ± 2.4 nm, respectively.

The molecular characteristics of single silk fiber, silk fibroin solution, silk fibroin films, and silk fibroin nanoparticles were investigated by means of ATR FT-IR microspectroscopy. This technique elucidates the secondary structure changes in silk fibroin during the preparation of silk fibroin nanoparticles and gives the molecular characteristics of native single silk fiber without sample destruction and short time analysis. From the studies of silk fibroin nanoparticles, it is concluded that the secondary structure of silk fibroin nanoparticles precipitated in methanol were rich in β -sheet structure, while silk fibroin nanoparticles precipitated in *iso*-propanol were rich in random coil structure. The secondary structures of silk fibroin films (untreated with organic solvent) have random coil structure. Therefore, the secondary structure of silk fibroin was controlled by organic solvent. From the studies of single silk fiber, it is concluded that the secondary structure of degummed silk fiber has crystalline structure more than that of virgin silk fiber.

For the deposition of silver nanoparticles on silk fibroin nanoparticles, silver nanoparticles can disperse and deposit on silk fibroin nanoparticles, which observed from TEM images. UV-Visible spectroscopy indicated that silver nanoparticles could deposit on silk fibroin nanoparticles, which observed from the decreasing absorption spectra of silver nanoparticles colloidal solution after silver nanoparticles are added

into the solution of silk fibroin nanoparticles. From the ATR FT-IR microspectroscopy, silver nanoparticles could be inserted between the β -sheet structures of silk fibroin structure. The crystalline structure of silk fibroin is reduced after silver nanoparticles deposition.



ศูนย์วิจัยทรัพยากร
จุฬาลงกรณ์มหาวิทยาลัย

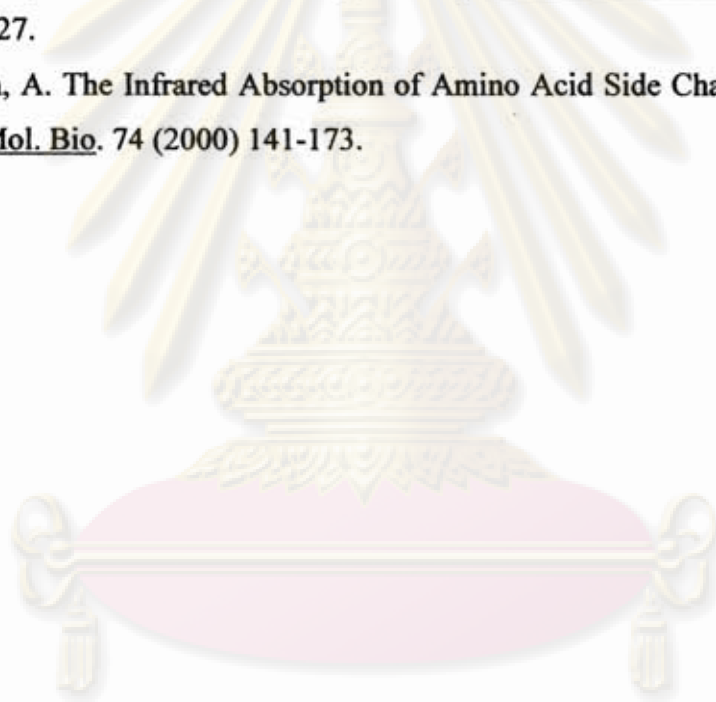
REFERENCES

- [1] Sashina, E.S.; Bocheks, A.M.; Novoselov, N.P.; and Kirichenko, D.A. Structure and Solubility of Natural Silk Fibroin. J. Appl. Chem. 79 (2006): 869-876.
- [2] Gil, E.; Frankowski, D.; and Hudson, S. Silk Fibroin Membrane from Solvent-Crystallized Silk Fibroin/Gelatin Blends: Effect of Blend and solvent Composition. J. Mater. Sci. Eng. 27 (2007): 426-431.
- [3] Ha, S.; Tonelli, A; and Hudson, S. Structural Studies of *Bombyx mori* Silk Fibroin during Regeneration from Solutions and Wet Fiber Spinning. Biomacromolecules 6 (2005): 1722-1731.
- [4] Sonthisombat, A.; and Speakman, P. Silk: Queen of fibres - the concise story. p.1-28. Cited in Sandoz colour chronicle. October/December 1990, p.1-4 and 16-19.
- [5] Seidman, L. Chapter 2: Protein structure. [online]. Available from: <http://matchmadison.edu/biotech/resources/proteins/labManual/chapter2.html>.
- [6] Zhang, Y.; Shen, W.; and Xiang, R. Formation of Silk Fibroin Nanoparticles in Water-miscible Organic Solvent and their Characterization. J. Nanopart. Res. 9 (2007): 885-900.
- [7] Raghava, G.P.S.; and Kaur, H. A server for β -turn types prediction. [online]. Available from: www.imtech.res.in/raghava/beteturns/turn.html.
- [8] Moniz, M. Structure and function of macromolecules. [online]. Available from: www.langara.bc.ca/biology/mario/Biol1115notes/biol1115chap5.html.
- [9] Zhang, H.; Magoshi, J; and Becker, M. Thermal Properties of *Bombyx mori* Silk Fibers. J. Appl. Polym. Sci. 86 (2002): 1817-1820.
- [10] Robson, R.M. In Silk; Composition, Structure and Properties. Handbook of Fibre Science and Technology, Volume 4. New York: 1985.
- [11] Tao, W.; Li, M.; and Zhao, C. Structure and Properties of Regenerated *Antheraea pernyi* Silk Fibroin in Aqueous Solution. Int. J. Biol. Macromol. 40 (2007): 472-478.
- [12] Wang, X.; Wenk, E.; and Matsumoto. A. Silk Microspheres for Encapsulation and Controlled Release. J. Control. Release. 117 (2007): 360-370.

- [13] Hino, T.; Tanimoto, M.; and Shimabayashi, S. Change in Secondary Structure of Silk Fibroin During Preparation of Its Microspheres by Spray-drying and Exposure to Humid atmosphere. *J. Colloid Interf Sci.* 226 (2003): 68-73.
- [14] Tsubouchi, K. Process for preparing fine powder of silk fibroin. US Patent 5853764, 1998.
- [15] Yeo, J.; Lee, K.; and Lee, Y. Silk Preparation and Characteristics of Silk Fibroin Microsphere. *Eur. Polym. J.* 39 (2003): 1195-1199.
- [16] Nam, J.; and Park, Y. Morphology of Regenerated Silk Fibroin: Effects of freezing Temperature, Alcohol Addition, and Molecular weight. *J. Appl. Polym. Sci.* 81 (2001): 3008-3021.
- [17] Li, Y.; Yuen, C.W.M. and Cheng, Y.F. Analysis of the Structural Characteristics of Silk Nanoscale Silk Particles. *J. Appl. Polym. Sci.* 100 (2006): 268-274.
- [18] Pellerin, C.; and Rousseau, M. Study of Molecular Orientation by Vibrational Spectroscopy: From Polymers to Silk. *Macromol.* 220 (2005): 85-98.
- [19] Image Library of Biological Macromolecules. Determination of Secondary Structure in Proteins by Fourier Transform Infrared (FT-IR) Spectroscopy. [online]. Available from: www.imb-jena.de/imglibdoc/ftir/image_ftir.html.
- [20] Shao, J.; Zheng, J.; Liu, J.; and Carr, C.M. Fourier Transform Raman and Fourier Transform Infrared Spectroscopy Studies of Silk Fibroin. *J. Appl. Polym. Sci.* 96 (2005): 1999-2004.
- [21] Urban, M. W. Attenuated Total Reflectance Spectroscopy of Polymer: Theory and Practice. Washington: American Chemical Society, 1996.
- [22] Do, T. T.; Celina, M.; and Fredericks, P. Attenuated Total Reflectance Infrared Microspectroscopy of Aged Carbon-filled Rubbers. *Polym. Degrad. Stab.* 77 (2002): 417-422.
- [23] Thongnopkun, P.; and Ekgasit, S. Attenuated Total Reflection Fourier Transform Infrared Spectra of Faceted Diamonds. *Anal. Chem.* 576 (2006): 130-135.
- [24] Ekgasit, S. ATR Spectral Intensity: What is the Upper Limit of Weak Absorption?. *Appl. Spectrosc.* 54 (2000): 756-760.
- [25] Ekgasit, S.; and Padermshoke, A. Optical contact in ATR/FT-IR Spectroscopy. *Appl. Spectrosc.* 55 (2001): 1352-1359.
- [26] Harrick, N. J. Internal reflection spectroscopy New York: Harrick Scientific Corporation, 1987.

- [27] Kim, U.; Park, J.; and Kim, J.H. Three-dimensional Aqueous-derived Biomaterial Scaffolds from Silk Fibroin. Biomaterials 26 (2005): 2775-2785.
- [28] Wang, X.; Kim, H.J.; and Xu, P. Biomaterial Coatings by Stepwise Deposition of Silk Fibroin. Langmuir 21 (2005): 11335-11341.
- [29] Grath, K.; and Kaplan, D. Protein-based materials. U.S.A.: Birkhäuser Boston, 1997.
- [30] Monti, P.; Freddi, G.; and Arosio, C. Vibrational Spectroscopic study of Sulphated Silk Proteins. J. Mol. Struct. 834-836 (2007): 202-206.
- [31] Socrates, G. Infrared and Raman Characteristic Group Frequencies Table and Charts. Chichester: John Wiley & Sons, 2001.
- [32] Griebenow, K.; Santos, A.; and Carrasquillo, K. Secondary Structure of Proteins in the Amorphous Dehydrated State Probed by FT-IR Spectroscopy, first ed., Internet J. Vibrational Spec., Vol.3.
- [33] Chalmers, J.M.; and Griffiths, P.R. Handbook of Vibrational Spectroscopy Volume 2. UK: John Wiley & Sons, 2002.
- [34] Kong, J.; and Yu, S. Fourier Transform Infrared Spectroscopic Analysis of Protein Secondary Structures. Acta Bioch. Bioph. Sin. 39 (2007):549-559.
- [35] Panayiotou, H.; and Kokot, S. Matching and Discrimination of Single Human-Scalp Hairs by FT-IR Micro-Spectroscopy and Chemometrics. Anal. Chim. Acta. 392 (1999): 223-235.
- [36] Dong, Q.; Su, H.; and Zhang, D. In situ depositing silver nanoclusters on silk fibroin fibers supports by a novel biotemplate redox technique at room temperature. J. Phys. Chem. B 109 (2005):17429-17434.
- [37] Asai, M.; Tsuboi, M.; and Shimanouchi, T. Infrared spectra of polypeptides and related compounds. J. Phys. Chem. 59 (1955): 322-325.
- [38] Hu, X.; Kaplan, D.; and Cebe, P. Determining Beta-Sheet Crystallinity in Fibrous Proteins by Thermal Analysis and Infrared Spectroscopy. Macromol. 39 (2006): 6161-6170.
- [39] Teramoto, H.; and Miyazawa, M. Molecular Orientation Behavior of Silk Sericin Film as Revealed by ATR Infrared Spectroscopy. Biomacromolecules 6 (2005): 2049-2057.

- [40] Mauerer, A.; and Lee, G. Changes in the Amide I FT-IR bands of Poly-L-lysine on Spray-drying from α -helix, β -sheet or Random coil conformations. J. Pharm. Biopharm. 62 (2006): 131-142.
- [41] Goormaghtigh, E.; Cabiaux, V.; and Ruyschaert, J. Secondary Structure and Dosage of Soluble and Membrane Proteins by Attenuated Total Reflection Fourier-transform Infrared Spectroscopy on Hydrated Films. Eur. J. Biochem. 193 (1990): 409-420.
- [42] Taketani, I.; Nakayama, S.; and Nagare, S. The Secondary Control of Silk Fibroin Thin Films by Post Treatment. Appl. Surf. Sci. 244 (2005): 623-626.
- [43] Hofmann, S.; Wong Po Foo, C.T.; and Rossetti, F. Silk fibroin as an Organic Polymer for Controlled Drug Delivery. J. Control. Release. 111 (2006): 219-227.
- [44] Barth, A. The Infrared Absorption of Amino Acid Side Chains. Prog. Biophys. Mol. Bio. 74 (2000) 141-173.



ศูนย์วิทยทรัพยากร
จุฬาลงกรณ์มหาวิทยาลัย

CURRICULUM VITAE

Name: Miss Kanjana Uthaichay

Date of Birth: May 13, 1982 **Birth place:** Chonburi, Thailand

Address: 1596/513 Samrong-nuea, Mueang, Samutprakarn, Thailand,
E-mail address: kae_m2on@hotmail.com

Education:

2004 Bachelor of Engineering (Petrochemicals and Polymeric Materials), Silpakorn University, Nakornpathom, Thailand

2008 Master of Science (Petrochemistry and Polymer Science), Chulalongkorn University, Bangkok, Thailand

Conferences:

March 2007 The 15th Academic Conference, the 2007 Annual Meeting, Faculty of Science, Chulalongkorn University, Thailand

May 2007 Polymer Graduate Conference of Thailand, Faculty of Science, Mahidol University, Thailand

October 2007 The 33rd Congress on Science and Technology of Thailand (STT.33) Walailak University, Nakorn Si Thammarat, Thailand

September 2007 National Research Council of Thailand, Thailand Research Expo, Central World Plaza, Bangkok, Thailand

December 2007 International Graduate Congress 2007, 3rd MPSGC, Faculty of Science, University of Malaya, Kuala Lumpur, Malaysia

March 2008 The 16th Academic Conference, the 2008 Annual Meeting, Faculty of Science, Chulalongkorn University, Thailand